JCI The Journal of Clinical Investigation

# IRE1α regulates skeletal muscle regeneration through Myostatin mRNA decay

Shengqi He, … , Zhenji Gan, Yong Liu

*J Clin Invest.* 2021. https://doi.org/10.1172/JCI143737.

**Research** In-Press Preview **Muscle biology**

## Graphical abstract

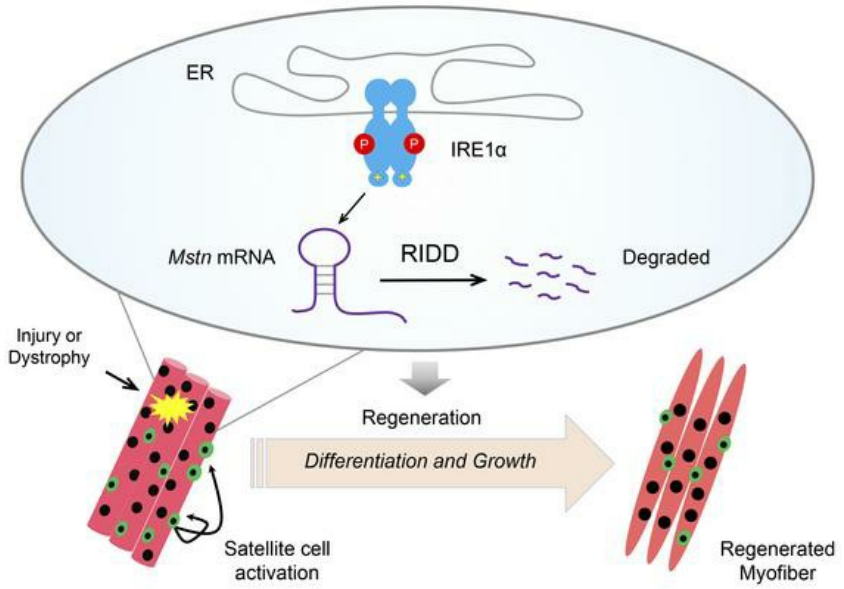

**IRE1α regulates skeletal muscle regeneration through Myostatin mRNA decay**

Shengqi He[1], Tingting Fu[2], Yue Yu[3], Qinhao Liang[1], Luyao Li[1], Jing Liu[2], Xuan Zhang[1], Qian Zhou[2], Qiqi Guo[2], Dengqiu Xu[2], Yong Chen[1], Xiaolong Wang[4], Yulin Chen[4], Jianmiao Liu[5], Zhenji Gan[2, *] and Yong Liu[1, *]

[1]Hubei Key Laboratory of Cell Homeostasis, College of Life Sciences; the Institute for Advanced Studies; Frontier Science Center for Immunology and Metabolism; Wuhan University, Wuhan, China

[2]State Key Laboratory of Pharmaceutical Biotechnology and MOE Key Laboratory of Model Animals for Disease Study, Department of Spine Surgery, Nanjing Drum Tower Hospital, The Affiliated Hospital of Nanjing University Medical School, Jiangsu Key Laboratory of Molecular Medicine, Chemistry and Biomedicine Innovation Center (ChemBIC), Model Animal Research Center, Nanjing University Medical School, Nanjing University, Nanjing, China

[3]Division of Ophthalmology, Beth Israel Deaconess Medical Center, Boston, Massachusetts, USA

[4]Key Laboratory of Animal Genetics, Breeding and Reproduction of Shaanxi Province, College of Animal Science and Technology, Northwest A&F University, Yangling, China

[5]Cellular Signaling Laboratory, Key Laboratory of Molecular Biophysics of Ministry of Education, Huazhong University of Science and Technology, Wuhan, China

[*]To whom correspondence should be addressed:

Yong Liu, Ph.D.

College of Life Sciences, Wuhan University

299 Bayi Road, Wuhan 430072, China

E-mail: liuyong31279@whu.edu.cn

Telephone: +86-27-68753463

Zhenji Gan, Ph.D.

Model Animal Research Center of Nanjing University

12 Xuefu Road

Pukou, Nanjing 210061, China

E-mail: ganzj@nju.edu.cn

Tel: 86-25-58641546

Fax: 86-25-58641500

Conflicts of Interest: The authors have declared that no conflict of interest exists.

**Abstract**

Skeletal muscle can undergo a regenerative process from injury or disease to preserve muscle mass and function, which is critically influenced by cellular stress responses. Inositol-requiring enzyme 1 (IRE1) is an ancient endoplasmic reticulum (ER) stress sensor and mediates a key branch of the unfolded protein response (UPR). In mammals, IRE1α is implicated in the homeostatic control of stress responses during tissue injury and regeneration. Here, we show that IRE1α serves as a myogenic regulator in skeletal muscle regeneration in response to injury and muscular dystrophy. We found in mice that IRE1α was activated during injury-induced muscle regeneration, and muscle-specific IRE1α ablation resulted in impaired regeneration upon cardiotoxin-induced injury. Gain- and loss-of-function studies in myocytes demonstrated that IRE1α acts to sustain both differentiation in myoblasts and hypertrophy in myotubes through regulated IRE1-dependent decay (RIDD) of mRNA encoding Myostatin, a key negative regulator of muscle repair and growth. Furthermore, in the mouse model of Duchenne muscular dystrophy (DMD), loss of muscle IRE1α resulted in augmented Myostatin signaling and exacerbated the dystrophic phenotypes. Thus, these results reveal a pivotal role for the RIDD output of IRE1α in muscle regeneration, offering insight into potential therapeutic strategies for muscle loss diseases.

## Introduction

The endoplasmic reticulum (ER) is an essential membrane network that governs the folding and secretion of nearly one third of the cellular proteome in eukaryotes. Increased protein folding demand or accumulation of unfolded/misfolded proteins within the ER lumen causes ER stress, activating the adaptive cell response termed unfolded protein response (UPR) (1-3). Among the three ER-resident transmembrane UPR sensors (3), inositol-requiring enzyme 1 (IRE1) is the most conserved signal transducer with dual enzyme activities, i.e. Ser/Thr protein kinase and endoribonuclease (RNase), within its cytoplasmic portion (1, 2, 4). Upon ER stress, IRE1 is activated through dimerization/oligomerization and autophosphorylation, mediating a key branch of the UPR signaling through its RNase activity (1-3, 5, 6). Activated IRE1 catalyzes the unconventional splicing of the mRNA encoding the transcription factor X-box binding protein 1 (XBP1) to generate a spliced active form of XBP1 (XBP1s), thereby driving a major UPR program involved in modulating protein folding, secretion and ER-associated degradation (ERAD) (5, 6). In addition, IRE1 can also directly degrade select mRNA species in a process referred to as "regulated IRE1-dependent decay" (RIDD) (7-9). In mammals, IRE1α signaling has been implicated in regulating a wide range of biological processes including determination of cell fate, metabolic homeostasis, and immune responses (10-14). Whereas XBP1s serves as a crucial effector of IRE1α's RNase activation, recent studies have also revealed implications of its RIDD activity in the control of secretory cargo proteins (8, 15), insulin production in pancreatic β-cells (16), hepatic lipid metabolism (17), and dendritic cell homeostasis in immunity (18). Moreover, a growing body of evidence suggests that dysregulated activation of IRE1α contributes

to the pathogenesis of many chronic diseases, including metabolic disorders, cancer, and neurodegeneration (1, 11, 19-22).

Skeletal muscles have the remarkable capacity to undergo regenerative growth in response to injury or other external stimuli. Muscle repair is a highly-coordinated process involving muscle damage, regeneration, and myofiber remodeling (23-25). Muscle regeneration relies on activation and expansion of myogenic stem cells, known as satellite cells, residing beneath the basal lamina of myofibers, followed by myoblast differentiation and ultimate fusion into multinucleated myotubes (26-28). At the final stage of muscle repair, myotubes undergo hypertrophy remodeling to generate mature muscle fibers and restore their contractile capacity. Multiple myogenic signaling pathways serve to control muscle regeneration and hypertrophy (27-29), mainly mediated by orchestrated activation of the transcriptional regulatory factors MYF5, MyoD and Myogenin, along with regulated expression of the myosin heavy chain (MyHC) genes (27, 28). In addition, a number of cytokines and growth factors are known to be critically involved in controlling muscle repair and growth, as exemplified by interleukin-6, myostatin/TGFβ, and insulin-like growth factor-1 (IGF1) (30, 31). Impairment of muscle regeneration and growth leads to muscle atrophy or dystrophy, which represents a key pathological feature of many human diseases with muscle loss (32). For instance, Duchenne muscular dystrophy (DMD), caused by mutations in the X-linked gene dystrophin, is the most common and severe form of human muscular dystrophy that remains incurable to date (33, 34). A better understanding of the complex interplays between the intrinsic cell signaling network and microenvironmental cues will uncover the molecular regulatory mechanisms in the maintenance of muscle mass, thus facilitating the development of regenerative therapeutics for muscle degeneration disorders.

As a critical regulator of ER stress response in restoring the proteostatic homeostasis, IRE1α has been documented to promote cell proliferation during the reparative regeneration of the liver (35) and the compensatory growth of pancreatic islets under metabolic stress (36). However, it has yet to be explored whether IRE1α plays a role in sensing skeletal muscle stress and regulating its regeneration process. In this study, we utilized cardiotoxin (CTX)-induced acute muscle injury model as well as the genetic *mdx* model of DMD in mice, and found that IRE1α acts to sustain muscle repair and growth, largely through its RIDD activity to downregulate the expression of the mRNA encoding Myostatin, a critical negative regulator of muscle regeneration and growth. Our findings demonstrate the physiological importance of IRE1α's RIDD activity in the control of muscle regeneration, and its dysregulation may represent an unrecognized mechanism linking ER stress to muscle degenerative diseases.

## Results

***Activation of the IRE1α signaling branch is implicated in skeletal muscle regeneration.*** To investigate whether IRE1α is implicated in regulating muscle regeneration, we first examined its activation states during the regenerative response to acute skeletal muscle injury via injecting CTX into the tibialis anterior (TA) muscles of adult mice. In line with previously reported findings (37), CTX-induced myofiber degeneration triggered robust muscle regeneration responses, as indicated by prominently elevated expression of embryonic MyHC (eMyHC) at 2 days post CTX treatment (Figure 1A). Starting at 2 days following CTX-elicited injury, we observed significant increases in the phosphorylation at $Ser^{724}$ within the kinase domain of IRE1α that peaked at 4 and 8 days (Figure 1A). Consistent with activated IRE1α's RNase activity, significantly increased *Xbp1* mRNA splicing and decreased abundance of *Blos1* mRNA, a typical RIDD substrate of IRE1α, were detected during the regenerative response to CTX-induced injury (Figure 1B), in parallel with marked activation of the *Myog* and *Myh8* gene expression program (Figure 1C). Notably, increased eIF2α phosphorylation and BiP protein expression levels were also seen following CTX treatment (Figure 1A). These results indicate that the IRE1α branch of the UPR is activated in response to muscle damage, and suggest that IRE1α may act as a component in the control mechanism during muscle repair and regenerative growth response.

To determine the importance of IRE1α in skeletal muscle regeneration, we employed the *Ern1*$^{f/f}$ mice with two *lox-P* sites flanking the exon 2 of the *Ern1* gene (38) and *Myod1-Cre* mice to generate skeletal muscle-specific IRE1α-knockout (referred to as *Ern1*$^{f/f}$*;Myod1-Cre*) mice, which were born at normal Mendelian ratios

and appeared to be grossly normal. Immunoblot analysis showed substantial reductions in IRE1α protein levels from multiple muscle types in *Ern1$^{f/f}$;Myod1-Cre* mice relative to their *Ern1$^{f/f}$* littermates or *Myod1-Cre* controls, whereas no changes were detected in their hearts (Supplemental Figure 1A). As expected, markedly reduced *Xbp1* mRNA splicing was detected in the *Ern1$^{f/f}$;Myod1-Cre* muscles relative to their control groups (Supplemental Figure 1B). *Ern1$^{f/f}$;Myod1-Cre* mice exhibited no overt differences in their body weight, muscle weight or myofiber morphology (Supplemental Figure 2A-D), and showed no significant alterations in the abundance of *Atf4* or *Chop* mRNA (Supplemental Figure 2E), or that of *Myh1*, *Myh2* or *Myh4* mRNA (Supplemental Figure 2F) in their TA muscles. This suggests that ablation of IRE1α neither provokes ER stress, nor affects muscle development. When subjected to CTX-induced injury in their TA muscles, animals of all three genotypes showed markedly reduced TA muscle weight, presumably due to extensive myofiber degeneration, at 4 days post CTX injection (Figure 1D). Whereas gradual restoration of TA muscle mass was seen in all three genotypes at 8 and 12 days after CTX injection (Figure 1D), a significant reduction in the weight of regenerating TA muscle was observed in *Ern1$^{f/f}$;Myod1-Cre* mice relative to their *Ern1$^{f/f}$* or *Myod1-Cre* counterparts at 12 days following CTX-induced injury (Figure 1D). This indicates that loss of IRE1α in muscle cells resulted in impaired regenerative response to acute muscle injury. Indeed, histological analysis revealed that at 8 days following CTX injection, while TA muscles from all three genotypes showed newly formed myofibers containing centralized nuclei that replaced the damaged myofibers (Figure

1E), significantly lower percentage of large regenerated myofibers was found in *Ern1*$^{f/f}$*;Myod-Cre* TA muscles than those of *Ern1*$^{f/f}$ or *Myod1-Cre* control mice at 8 or 12 days after CTX-induced injury (Figure 1E and 1F; Supplemental Figure 3A). This defect of reparative regeneration in *Ern1*$^{f/f}$*;Myod1-Cre* TA muscles was further reflected by analysis of muscle sections stained for eMyHC (Figure 1G and 1H; Supplemental Figure 3B). At 8 days following CTX injection, whereas *Ern1*$^{f/f}$ or *Myod1-Cre* TA muscles exhibited strongly expressed eMyHC in most myofibers, *Ern1*$^{f/f}$*;Myod1-Cre* TA muscles showed marked reductions in eMyHC expression in many myofibers, along with eMyHC-positive fibers displaying apparent heterogeneity in size (Figure 1 G and 1H). At 12 days after CTX injection, however, *Ern1*$^{f/f}$ or *Myod1-Cre* TA muscles had weaker eMyHC signals and larger myofibers, but *Ern1*$^{f/f}$*;Myod1-Cre* TA muscles displayed accumulation of eMyHC in smaller myofibers, likely reflecting an earlier stage of delayed regeneration (Supplemental Figure 3B). Thus, loss of muscle IRE1α leads to impaired skeletal muscle regeneration after acute injury.

Skeletal muscle regeneration in response to injury involves highly orchestrated myogenic transcriptional network and cytokine signaling. Interestingly, we detected markedly decreased *Xbp1* mRNA splicing but significantly increased abundance of *Mstn* mRNA encoding Myostatin (Figure 1I), along with a considerable reduction in *Igf1* mRNA expression (Supplemental Figure 3C), in TA muscles of *Ern1*$^{f/f}$*; Myod1-Cre* mice relative to their *Ern1*$^{f/f}$ counterparts during the regenerative response at 4 and 8 days after CTX injection. Given that Myostatin is a secreted TGFβ family

member protein that functions as a potent negative regulator of myogenic differentiation and muscle growth (30), this suggests that IRE1α ablation affected the signaling pathways in the control of muscle regeneration. Indeed, we observed prominently elevated phosphorylation of Smad3, the downstream transcription factor of the Myostatin signaling cascade (39), in *Ern1$^{f/f}$;Myod1-Cre* TA muscles (Figure 1J). In accordance with poorer muscle regeneration, this enhanced Myostatin signaling was associated with marked reductions in eMyHC protein levels (Figure 1J). Together, these results demonstrate that IRE1α abrogation leads to impaired muscle regeneration and enhanced Myostatin signaling in response to acute muscle injury, indicating that IRE1α may function as a myogenic regulator of muscle repair and growth.

***IRE1α RNase regulates Myostatin expression and myoblast differentiation.*** Because skeletal muscle regeneration involves the activation, proliferation and differentiation of muscle satellite cells (MuSCs) (28), we first examined whether IRE1α ablation affected MuSCs in *Ern1$^{f/f}$;Myod1-Cre* mice. Using a fluorescence-activated cell sorting (FACS)-based method (40) for quantitative analysis of either quiescent or activated MuSCs (VCAM1$^{+}$CD45$^{-}$CD31$^{-}$Sca1$^{-}$ cells), we observed no significant differences in the amount of muscle satellite cells from CTX-injured TA muscles of *Ern1$^{f/f}$*, *Myod1-Cre* or *Ern1$^{f/f}$;Myod1-Cre* mice (Supplemental Figure 4A and 4B). This suggests that the satellite cell niche was presumably not affected by muscle IRE1α deficiency. We then investigated the requirement for IRE1α in myogenesis

using primary myoblasts isolated from *Ern1*$^{f/f}$*;Myod1-Cre* and *Myod1-Cre* mice. During the early period of myoblast differentiation into myotubes, we observed significantly induced IRE1α phosphorylation (Figure 2A and 2B), in parallel with increased *Xbp1* mRNA splicing and markedly induced *Myh4* expression (Supplemental Figure 5A). Consistently, loss of IRE1α in primary myoblasts resulted in significantly upregulated expression of *Mstn* mRNA (Figure 2C), along with elevated Smad3 phosphorylation and reduced MyHC protein level (Figure 2D and 2E). At 3 days after differentiation, increased Myostatin protein was detected in the culture medium of *Ern1-mKO* myotubes (Figure 2F); and most *Myod1-Cre* myoblasts became elongated and fused with expression of the differentiation marker MyHC (Figure 2G-2I). By contrast, *Ern1-mKO* myoblasts showed significant decreases in cell fusion and multinuclear myotube formation (Figure 2G-2I), with fewer and shorter myotubes observed after differentiation for 5 days (Supplemental Figure 5B). Moreover, *Ern1-mKO* myocytes had significant reductions in the mRNA and protein expression levels of the differentiation markers Myogenin and MyHC when compared to their *Myod1-Cre* control (Figure 2J-2L). These results suggest that IRE1α ablation leads to upregulation of Myostatin expression and impairment of myoblast differentiation in a cell-autonomous manner.

To further test whether IRE1α's RNase activity is required for myoblast differentiation, we examined the effects of restored expression of wild-type (WT) or mutant IRE1α using adenoviruses upon the defective differentiation of *Ern1-mKO* myoblasts. Immunostaining of MyHC showed that overexpression of IRE1α-WT

effectively restored the differentiation capacity (Figure 3A and 3B) as well as the protein and mRNA expression levels of *Myog* and *Myh4* in *Ern1-mKO* myoblasts (Figure 3C-F) to an extent similar to that of *Myod1-Cre* controls, whereas overexpression of the IRE1α kinase-dead (KD, K599A) or RNase-defective (RD, K907A) mutant versions (41) lost these effects (Figure 3A-F). Supporting the role of IRE1α in suppression of Myostatin, overexpression of IRE1α-WT, but not its kinase- or RNase-deficient mutants, substantially blunted the upregulated expression of *Mstn* in *Ern1-mKO* myocytes, which resembled the changes of the typical RIDD substrate, *Blos1* (Figure 3F). Notably, adenoviral overexpression of *XBP1s* did not significantly affect the differentiation capacity or *Mstn* expression in *Ern1-mKO* myocytes (Figure 3A-F). These data demonstrate an IRE1α RNase-dependent, XBP1-independent regulation of myoblast differentiation, suggesting that IRE1α acts as a negative regulator of Myostatin to control myoblast differentiation during muscle regeneration.

***IRE1α downregulates Myostatin expression and promotes myotube hypertrophy.*** Because Myostatin is also known as an autocrine factor to suppress hypertrophy in myotubes (30, 42, 43), we next tested if IRE1α could impact myotube hypertrophy remodeling through downregulating Myostatin expression. In differentiated C2C12 myotubes, adenoviral expression of a short hairpin RNA (shRNA) directed against IRE1α (Sh-Ern1), in comparison to the scramble shRNA control (Sh-Con), resulted in substantially decreased *Xbp1* mRNA splicing, but significantly increased mRNA abundance of *Blos1* and *Mstn* (Figure 4A), which was accompanied by a significant reduction in the mRNA level of *Myh4* but not *Igf1* (Figure 4A). In line with enhanced Myostatin signaling and impaired myotube growth, knockdown of IRE1α expression

led to significantly higher production of Myostatin protein in the medium (Figure 4B) and increased phosphorylation of Smad3 (Figure 4C), along with decreases in S6K phosphorylation and MyHC protein levels. Moreover, this was in parallel with significantly reduced diameters of myotubes (Figure 4D) and total cellular protein contents (Figure 4E). This is consistent with the phenotypes of smaller myofibers in mice with muscle IRE1α abrogation following CTX-induced injury. Conversely, when compared to the control, adenoviral IRE1α overexpression in differentiated C2C12 myotubes resulted in significantly elevated *Xbp1* mRNA splicing (Figure 4F), reduced mRNA abundance of *Blos1* and *Mstn* (Figure 4F), lower Myostatin protein production (Figure 4G) and signaling (Figure 4H), along with enlarged myotubes (Figure 4I) and higher cellular protein contents (Figure 4J). Notably, adenoviral shRNA knockdown of XBP1 expression caused a slight reduction in *Mstn* mRNA level (Supplemental Figure 6A), while showing no significant effect upon myotube growth (Supplemental Figure 6B). In addition, adenoviral overexpression of IRE1α-WT, but not its KD or RD mutant versions, significantly increased *Xbp1* mRNA splicing and decreased the mRNA abundance of *Mstn* and *Blos1* in C2C12 myotubes (Figure 4K). These in vitro analyses via loss- and gain-of-function strategies in myotubes strongly suggest that IRE1α downregulation of Myostatin expression also contributes to the control of myotube hypertrophy remodeling. Since Myostatin was reported to impact myoblast proliferation (44), we also evaluated whether IRE1α exerts a regulatory action in this regard. MTT analyses showed that neither IRE1α deficiency nor its overexpression had significant effects upon the proliferation rate of primary or C2C12 myoblasts (Supplemental Figure 7A-C). Moreover, FACS analyses showed that knockdown of IRE1α expression in C2C12 myoblasts did not affect cell death, which was increased upon differentiation stimuli

(Supplemental Figure 7D). Thus, IRE1α-directed regulation of Myostatin is implicated in both myocyte differentiation and hypertrophy growth, consistent with our observation in vivo that loss of IRE1α led to impairment in muscle regeneration upon injury.

***Myostatin mediates IRE1α's regulation of muscle cell differentiation and growth.*** We then determined whether Myostatin is required for IRE1α-mediated effect on myoblast differentiation using Mstn-KO C2C12 cells in which *Mstn* was abrogated by the CRISPR/Cas9-based strategy (45). Immunostaining of MyHC in differentiated myotubes showed slightly increased fusion index and myotube diameter in Mstn-KO cells relative to the wildtype (WT) control cells (Figure 5A-C). Whereas knockdown of IRE1α expression resulted in lower cell fusion and smaller myotube formation in parallel with higher Myostatin production (Figure 5D) in WT myoblasts, loss of Myostatin diminished these effects of IRE1α deficiency in *Mstn*-KO cells (Figure 5A-D). Consistently, immunoblotting and RT-PCR analyses showed that ablation of Myostatin restored the protein and mRNA expression of the myogenic markers Myogenin and MyHC in the face of IRE1α knockdown (Figure 5E-G), with no significant alterations observed in *Igf1* mRNA level (Figure 5G). Moreover, the promoting effects of IRE1α overexpression upon muscle cell differentiation and growth were also diminished in *Mstn*-KO cells (Supplemental Figure 8A-E). These data revealed the importance of Myostatin suppression, at least in large part, in mediating IRE1α regulation of myocyte differentiation and growth. Together, our results support a model in which IRE1α suppresses Myostatin expression, thereby promoting myoblast differentiation and myotube hypertrophy growth during skeletal muscle regeneration.

***Myostatin mediates IRE1α's regulatory action during skeletal muscle regeneration.*** To determine the importance of Myostatin in mediating IRE1α's regulatory effect in vivo upon muscle regeneration, we generated the recombinant adeno-associated virus 2/9 (AAV2/9) expressing the N-terminal propeptide (MyoPPT) of Myostatin, which is capable of inhibiting the biological activity and function of mature Myostatin (46-48). Systemic delivery of MyoPPT (49, 50) to neonatal *Ern1*$^{f/f}$ and *Ern1*$^{f/f}$*;Myod1-Cre* mice, relative to the GFP control, resulted in efficient MyoPPT expression in their TA muscles and did not influence IRE1α's *Xbp1* mRNA splicing activity (Figure 6A and 6B); and in accordance with reported findings (49, 50), blocking Myostatin signaling by MyoPPT caused significant increases in their body weight and TA muscle weight in both groups (Figure 6C and 6D). Importantly, at 8 days following CTX-induced injury, MyoPPT not only promoted the reparative regeneration of TA muscles of the *Ern1*$^{f/f}$ control group, but also prominently rescued the regenerative defect of *Ern1*$^{f/f}$*;Myod1-Cre* TA muscles, as evidenced by significantly increased TA muscle weight (Figure 6E), more newly formed myofibers containing centralized nuclei (Figure 6F), increased eMyHC expression (Figure 6G), and higher percentages of large regenerated myofibers (Figure 6H) and eMyHC-positive fibers (Figure 6I) when compared to the GFP control group (Figure 6E-I). These results further demonstrate in vivo that Myostatin is a crucial player in mediating IRE1α ablation-associated impairment of skeletal muscle regeneration upon acute injury.

***IRE1α suppresses Myostatin expression through its RIDD activity.*** We next asked if

the mRNA expression of *Mstn* is subjected to the control of IRE1α's RIDD activity. To determine if *Mstn* mRNA represents a valid RIDD substrate, we conducted bioinformatics analysis combined with prediction of mRNA secondary structures. Indeed, we identified a highly conserved region in mammalian mRNAs encoding Myostatin (spanning nucleotide 335 to 349 downstream of the putative transcription start site in mouse *Mstn* mRNA) which possesses the postulated RIDD consensus sequence (CNGCNN) (9) within a predicted hairpin structure containing a potential IRE1α cleavage site as found in *Xbp1* mRNA (Figure 7A). Then, we tested whether this region of *Mstn* mRNA could be directly cleaved by purified recombinant IRE1α protein, utilizing a synthetic 14-nucleotide *Mstn* mRNA molecule labeled with 5'-FAM fluorophore and 3'-black hole quencher (BHQ) as the substrate in an in vitro biochemical assay (Figure 7B). Incubation with IRE1α of this *Mstn* mRNA substrate abolished the quenching effect of BHQ, resulting in a dramatic increase in its fluorescent output signal (Figure 7B). By contrast, addition of 4μ8C, a pharmacologic inhibitor of IRE1α RNase activity (51, 52), markedly reduced this cleavage-based fluorescent signal (Figure 7B). To affirm IRE1α's action at the putative cleavage site, we generated a synthetic mutant *Mstn* mRNA substrate via replacing the conserved GC by CA, which completely abolished the cleavage-based fluorescent signal in comparison to its wild-type (WT) version (Figure 7B). Furthermore, quantitative RT-PCR analysis in HEK293T cells showed that co-transfected expression of IRE1α resulted in significantly decreased abundance of the WT but not the GC-to-CA mutant *Mstn* mRNA spanning the entire coding region of Myostatin (Figure 7C).

Interestingly, RT-PCR analyses showed that this *Mstn* mRNA could be immunoprecipitated along with the WT but not the truncation mutant IRE1α protein lacking its RNase domain from co-transfected HEK293T cells (Figure 7D); by contrast, deletion of the stem-loop structure of the *Mstn* mRNA abolished its ability to associate with IRE1α protein (Figure 7D). This indicates the structural involvement of IRE1α RNase domain and the stem-loop of the *Mstn* mRNA substrate in this particular RIDD machinery. We further determined if IRE1α could affect the stability of *Mstn* mRNA using C2C12 myotubes following treatment with Actinomycin D. Knockdown of IRE1α resulted in decreased degradation rate of *Mstn* mRNA (Figure 7E), whereas IRE1α overexpression significantly accelerated it (Figure 7F). Collectively, these results demonstrate that *Mstn* mRNA could indeed serve as a *bona fide* RIDD substrate of IRE1α.

We further validated that pharmacologic inhibition by 4μ8C of IRE1α RNase activity in primary myoblasts was able to, in a dose-dependent fashion, suppress *Xbp1* mRNA splicing and elevate the mRNA abundance of *Blos1* and *Mstn* (Figure 8A), leading to increased activation of Myostatin signaling, reduced protein expression of myogenic markers, and prominently lower myotube formation (Figure 8B-E). Consistently, 4μ8C inhibition of IRE1α RNase activity in differentiated C2C12 myotubes also resulted in decreased *Xbp1* mRNA splicing and elevated mRNA abundance of *Mstn* (Figure 8F), enhanced Myostatin signaling and lower levels of myogenic markers (Figure 8G) as well as decreased diameters of myotubes (Figure 8H and 8I). Together, these data clearly demonstrate that IRE1α could employ its

RNase-dependent RIDD activity to blunt the mRNA expression of Myostatin and exert its myogenic effect during the differentiation of myoblasts and hypertrophic growth of myotubes.

***Loss of IRE1α exacerbates the dystrophic phenotypes in mdx mice.*** DMD is the most common and severe form of muscular dystrophy and it remains incurable to date (33, 34). The *mdx* mouse model of DMD exhibits extensive muscle degeneration and regeneration due to a null mutation in the *Dmd* gene coding for the Dystrophin protein that causes higher sensitivity of myofibers to contractile stress (53). We wondered if the IRE1α-Myostatin regulatory circuit also plays a protective role in the setting of muscular dystrophy. To this end, we generated *mdx*/*Ern1*$^{f/f}$*;Myod1-Cre* mice with muscle-specific IRE1α deletion in the *mdx* background through genetic intercrossing. As expected, we detected significantly increased abundance of TA muscle *Mstn* mRNA as well as higher circulating Myostatin protein in *mdx/Ern1*$^{f/f}$*;Myod1-Cre* mice relative to their *mdx/Ern1*$^{f/f}$ littermates (Figure 9A and 9B). This was associated with elevated Smad3 phosphorylation and reduced eMyHC protein level (Figure 9C and 9D). Supporting a defective IRE1α-mediated suppression of Myostatin and weakened muscle regeneration, *mdx*/*Ern1*$^{f/f}$*;Myod1-Cre* mice at 6 weeks, as well as at 21 weeks, of age had grossly smaller gastrocnemius (Gas) and TA muscles, and the weight of these muscles was significantly lower than their *mdx*/*Ern1*$^{f/f}$ counterparts (Figure 9E and 9F; Supplemental Figure 9A). Histological analyses revealed more severe muscle dystrophic characteristics in *mdx*/*Ern1*$^{f/f}$*;Myod1-Cre* animals, as indicated by higher variations in their fiber size, apparently elevated number of small fibers, as well as more infiltration of inflammatory immune cells as a result of degenerated myofibers (Figure 9G; Supplemental Figure 9B). Immunostaining of

Laminin in muscle sections showed many smaller regenerating myofibers in Gas and TA muscles of *mdx*/*Ern1*$^{f/f}$*;Myod1-Cre* mice at 6 or 21 weeks of age than their *mdx*/*Ern1*$^{f/f}$ counterparts (Figure 9H; Supplemental Figure 9C), with significantly lower percentage of larger regenerating myofibers observed in TA muscles (Figure 9I; Supplemental Figure 9D). This indicates that loss of IRE1α results in impaired maturation of myofibers during the regenerative growth of *mdx*/*Ern1*$^{f/f}$*;Myod1-Cre* muscles, similar to its effect upon reparative muscle growth following CTX-induced acute injury. Utilizing Evans blue dye staining to assess the muscle fiber integrity, we further detected more pronounced damage with higher dye uptake in *mdx*/*Ern1*$^{f/f}$*;Myod1-Cre* muscles (Figure 9J and 9K). In addition, we observed no overt changes in the serum levels of creatine kinase (CK), a hallmark indicator of damaged muscles, in *Ern1*$^{f/f}$*;Myod1-Cre* mice, but found marked elevations in serum CK levels in *mdx*/*Ern1*$^{f/f}$ mice relative to their *Ern1*$^{f/f}$ controls (Figure 9L). Moreover, *mdx*/*Ern1*$^{f/f}$*;Myod1-Cre* mice displayed more pronounced increases in their serum CK levels relative to *mdx*/*Ern1*$^{f/f}$ mice (24109 ± 3797U/L versus 14437 ± 2719 U/L, n = 5 mice per genotype, p = 0.0013). To further evaluate the impact of IRE1α deficiency upon muscle functionality and performance, we challenged the animals with treadmill exercise and measured the running time and distance before exhaustion. Whereas *Ern1*$^{f/f}$*;Myod1-Cre* and *Ern1*$^{f/f}$ mice displayed no significant difference in their exercise performance, *mdx*/*Ern1*$^{f/f}$ animals showed a significantly shorter running time and distance (Figure 9M), and *mdx*/*Ern1*$^{f/f}$*;Myod1-Cre* mice exhibited a more pronounced impairment in their running ability (*mdx*/*Ern1*$^{f/f}$, 651 ± 88 m versus *mdx*/*Ern1*$^{f/f}$*;Myod1-Cre*, 364 ± 90 m, n = 5 mice per genotype, p = 0.004). Thus, these results demonstrate that ablation of IRE1α aggravates the severity of muscle dystrophy stemming from the lack of dystrophin in *mdx* mice, further establishing the

IRE1α-Myostatin axis as an important regulatory loop during regeneration in the setting of muscle dystrophy.

## Discussion

Skeletal muscle relies critically on its self-regeneration for preserving muscle mass and ensuring muscle function in response to injury and disease. Muscle regenerative capacity declines with age and is severely compromised in many muscular dystrophies (39). Delineation of the molecular mechanisms involved in regulating skeletal muscle regeneration and repair is of great importance to development of therapeutic approaches for muscle degenerative diseases. Herein, utilizing two mouse models, we have uncovered a critical role for the UPR sensor IRE1α in promoting skeletal muscle regeneration in response to CTX-induced acute muscle injury or genetic muscle dystrophy. Ablation of IRE1α specifically in skeletal muscles results in impaired muscle regenerative repair or worsened progression of muscle dystrophy. Importantly, our data demonstrate that IRE1α employs its RNase-dependent RIDD action to downregulate the level of mRNA encoding Myostatin, a key inhibitory regulator of muscle growth and repair. Our findings reveal a hitherto unrecognized physiological function of the RIDD output of IRE1α enzyme in the control of muscle regeneration and growth (Figure 10), suggesting that IRE1α may serve as an important modifier in the disease progression of muscular dystrophy or muscle loss.

IRE1α is the most ancient ER stress sensor that conveys a critical signaling response through its RNase activity to generate an active transcription factor XBP1s (3, 5) . While IRE1α is best known to exert its pro-survival actions through XBP1s when coping with ER stress, emerging lines of evidence also indicate that activated IRE1α RNase activity may have a broad range of functions, as reflected by an increasing amount of identified putative RIDD substrates (8, 15). However, the physiologically relevant RIDD actions of IRE1α have yet to be established in vivo. In this study, we provide physiological evidence for an RIDD-mediated mechanism by

which IRE1α regulates Myostatin production and regenerative maturation of myofibers in response to muscle injury or degenerative dystrophy. It is notable that ablation of IRE1α did not cause changes in muscle and myofiber sizes or Myostatin expression levels in *Ern1$^{f/f}$;Myod1-Cre* mice in the absence of injury or dystrophy. Moreover, IRE1α phosphorylation is relatively low in muscle cells under basal conditions, but is highly induced during myoblast differentiation or upon muscle injury. This suggests that activation of the IRE1α-Myostatin regulatory circuit is coupled to the stress condition induced by muscle injury or damage, conceivably reflecting the multi-task property of IRE1α in utilizing its RIDD activity to handle various types of stress conditions in a tissue- or cell type-specific fashion.

It is worth noting that we used *Myod1-Cre* mice for creating mice with IRE1α deletion specifically in skeletal muscles. Because of the activated expression pattern of *Myod1* during myogenesis (54), IRE1α abrogation most likely occurred in muscle stem cells (i.e. satellite cells) at particular differentiation stages as well as in mature muscle fibers. Our results from analyses of muscle cell differentiation and growth in vitro suggest that IRE1α can promote both myoblast differentiation and myotube hypertrophy growth. Thus, the impairment of injury-induced regeneration in *Ern1$^{f/f}$;Myod1-Cre* mice can be largely attributed to the cell-autonomous action of IRE1α in myocyte differentiation and growth. This is in accordance with the fact that myostatin can regulate both differentiation in myoblasts and hypertrophy in myotubes (55). Moreover, inhibition of Myostatin has been shown to improve the hallmarks of the muscular dystrophy in *mdx* mice (56, 57). This also supports our model that the lack of IRE1α-Myostatin regulatory axis contributes to the more severe dystrophic phenotypes in *mdx/Ern1$^{f/f}$;Myod1-Cre* mice.

XBP1 has been recently reported to be dispensable for satellite cell-mediated muscle regeneration, whereas the PERK/eIF2α arm of the UPR may play an important role in this process (58). Documented studies have also suggested that Myostatin can suppress satellite cell activation and self-renewal (43, 59, 60). While our results indicate that IRE1α deficiency caused no significant changes in the amount of TA muscle satellite cells upon acute injury, it has yet to be more thoroughly interrogated whether IRE1α can regulate satellite cells through a Myostatin-mediated mechanism or cell-intrinsically in an XBP1-independent manner, e.g. by affecting the STAT3 pathway (35, 61) that was reported to critically regulate the proliferation and self-renewal of muscle stem cells (62).

Myostatin, GDF11 and Activin A are the three circulating factors that belong to the TGFβ family in the negative control of skeletal muscle mass (30). It remains to be dissected if IRE1α also contributes in the regulation of GDF11 or Activin A production. In addition, despite that IRE1α did not directly, or through Myostatin signaling, affect the expression of IGF1, a potent inducer of muscle hypertrophy (30), in differentiated myotubes, and that XBP1s showed merely marginal effect on myotube growth in vitro, it warrants further investigating if IRE1α can simultaneously act to positively regulate *Igf1* expression through the XBP1s pathway in vivo.

In summary, our results have unmasked a crucial role of IRE1α in regulating skeletal muscle regeneration through RIDD control of Myostatin expression. Given its well-established central role in suppressing muscle regeneration and growth (30, 42, 43, 59, 60, 63-65), Myostatin has been shown to represent a valuable target for improving muscular dystrophy in mouse models. In this scenario, targeted modulation of the RIDD output of IRE1α may represent a potential avenue for therapeutic intervention in DMD or other skeletal muscle degenerative diseases.

## Methods

**Animal studies.** C57BL/6J mice were obtained from Shanghai Laboratory Animal Co. Ltd. Generation of *Ern1*$^{f/f}$ mice has been described previously in detail (38). *Ern1*$^{f/f}$ mice were intercrossed with mice expressing *Cre* recombinase under the control of a *Myod1* promoter (Jackson Laboratory, Stock No. 014140) to create mice with muscle-specific deletion of IRE1α. The *mdx* mice were purchased from the Jackson Laboratory (Stock No. 000476). Male *Ern1*$^{f/f}$ mice were first bred with homozygote female *Dmd*$^{mdx/mdx}$ mice to generate *Ern1*$^{f/+}$*;Dmd*$^{mdx/Y}$ males and *Ern1*$^{f/+}$*;Dmd*$^{mdx/+}$*females*. Male *Ern1*$^{f/+}$*;Dmd*$^{mdx/Y}$ mice were then bred to female *Dmd*$^{mdx/mdx}$ mice to generate *Ern1*$^{f/+}$*;Dmd*$^{mdx/mdx}$ females and *Ern1*$^{f/+}$*;Dmd*$^{mdx/Y}$ males, which were subsequently intercrossed to obtain *Ern1*$^{f/f}$*;Dmd*$^{mdx/mdx}$ *females*. Female *Ern1*$^{f/f}$*;Dmd*$^{mdx/mdx}$ mice were finally bred with male *Ern1*$^{f/f}$*;Myod1-Cre* mice to produce *Dmd*$^{mdx/Y}$/*Ern1*$^{f/f}$*;Myod1-Cre* or *Dmd*$^{mdx/Y}$/*Ern1*$^{f/f}$ males. Male offspring were genotyped, randomly assigned, and used at 5-21 weeks of age. Littermate controls were used in all cases, and histological analysis were performed by investigators who were blinded to the experimental groups.

Detailed methods are in the Supplemental Material.

**Statistics.** All data represent the mean ± SEM, with $P < 0.05$ considered to have a statistically significant difference. Differences between groups were tested using the unpaired two-tailed Student's *t* test, or by analysis of variance (ANOVA) with Bonferroni's post-hoc test when more than two groups were compared as indicated in the figure legends. All data points were used in statistical analyses. Statistical analyses were carried out using Prism 8 software (GraphPad).

**Study approval.** All animal studies were carried out in strict accordance with the Institutional Guidelines for the humane treatment of animals, and all experimental protocols were approved by both IACUC Committees at the College of Life Sciences, Wuhan University and the Model Animal Research Center (MARC) of Nanjing University.

## Author Contributions

S.H, Z.G and Y.L conceived and designed the studies. S.H performed most of the experiments and analyzed the data. T.F, Y.Y, Q.L, L.L, J.L, X.Z, Q.Z, Q.G, D.X, Y.C conducted some of the animal studies and cellular experiments. S.H, Z.G and Y.L analyzed data. X.W, Yulin C and Jianmiao L provided assistance with the experimental design, reagents and data analysis. S.H, Z.G and Y.L wrote the manuscript.

## Acknowledgements

Special thanks to Dr. Dahai Zhu from Chinese Academy of Medical Sciences and Dr. Zhen-Guo Wu from Hong Kong University of Science & Technology for insightful discussions. This work was supported by grants from the Ministry of Science and Technology of China (National Key R&D Program of China 2018YFA0800700 and 2016YFA0500100) to Y.L and Z.G, and from the National Natural Science Foundation of China (No. 31690102, 91857204, 32021003, 31922033, 91857105, 31771291 and 91739303) to YL, Z.G and Jianmiao L. Supported also by Natural Science Foundation of Jiangsu Province (BK20170014) to Z.G, and Fundamental Research Funds for the Central Universities (021414380511 and 2042020kf1056) to Z.G and Y.L.

## References


1. Hetz C, and Glimcher LH. Protein homeostasis networks in physiology and disease. *Current opinion in cell biology.* 2011;23(2):123-5.
2. Schroder M, and Kaufman RJ. The mammalian unfolded protein response. *Annual review of biochemistry.* 2005;74(739-89.
3. Walter P, and Ron D. The unfolded protein response: from stress pathway to homeostatic regulation. *Science.* 2011;334(6059):1081-6.
4. Cox JS, Shamu CE, and Walter P. Transcriptional induction of genes encoding endoplasmic reticulum resident proteins requires a transmembrane protein kinase. *Cell.* 1993;73(6):1197-206.
5. Han J, and Kaufman RJ. Physiological/pathological ramifications of transcription factors in the unfolded protein response. *Genes Dev.* 2017;31(14):1417-38.
6. Yoshida H, Matsui T, Yamamoto A, Okada T, and Mori K. XBP1 mRNA is induced by ATF6 and spliced by IRE1 in response to ER stress to produce a highly active transcription factor. *Cell.* 2001;107(7):881-91.
7. Hollien J, Lin JH, Li H, Stevens N, Walter P, and Weissman JS. Regulated Ire1-dependent decay of messenger RNAs in mammalian cells. *J. Cell Biol.* 2009;186(3):323-31.
8. Hollien J, and Weissman JS. Decay of endoplasmic reticulum-localized mRNAs during the unfolded protein response. *Science.* 2006;313(5783):104-7.
9. Oikawa D, Tokuda M, Hosoda A, and Iwawaki T. Identification of a consensus element recognized and cleaved by IRE1 alpha. *Nucleic acids research.* 2010;38(18):6265-73.
10. Hetz C, and Papa FR. The Unfolded Protein Response and Cell Fate Control. *Mol. Cell.* 2018;69(2):169-81.
11. Hetz C. The unfolded protein response: controlling cell fate decisions under ER stress and beyond. *Nature reviews. Molecular cell biology.* 2012;13(2):89-102.

12. Hotamisligil GS. Endoplasmic reticulum stress and the inflammatory basis of metabolic disease. *Cell.* 2010;140(6):900-17.
13. Hetz C, Zhang K, and Kaufman RJ. Mechanisms, regulation and functions of the unfolded protein response. *Nature reviews. Molecular cell biology.* 2020;21(8):421-38.
14. Bettigole SE, and Glimcher LH. Endoplasmic reticulum stress in immunity. *Annual review of immunology.* 2015;33(107-38.
15. Maurel M, Chevet E, Tavernier J, and Gerlo S. Getting RIDD of RNA: IRE1 in cell fate regulation. *Trends in biochemical sciences.* 2014;39(5):245-54.
16. Lee AH, Heidtman K, Hotamisligil GS, and Glimcher LH. Dual and opposing roles of the unfolded protein response regulated by IRE1alpha and XBP1 in proinsulin processing and insulin secretion. *Proc. Natl. Acad. Sci. U. S. A.* 2011;108(21):8885-90.
17. So JS, et al. Silencing of lipid metabolism genes through IRE1alpha-mediated mRNA decay lowers plasma lipids in mice. *Cell Metab.* 2012;16(4):487-99.
18. Osorio F, et al. The unfolded-protein-response sensor IRE-1alpha regulates the function of CD8alpha+ dendritic cells. *Nature immunology.* 2014;15(3):248-57.
19. Zhao N, et al. Pharmacological targeting of MYC-regulated IRE1/XBP1 pathway suppresses MYC-driven breast cancer. *J. Clin. Invest.* 2018;128(4):1283-99.
20. Shan B, et al. The metabolic ER stress sensor IRE1alpha suppresses alternative activation of macrophages and impairs energy expenditure in obesity. *Nature immunology.* 2017;18(5):519-29.
21. Sha H, He Y, Yang L, and Qi L. Stressed out about obesity: IRE1alpha-XBP1 in metabolic disorders. *Trends Endocrinol. Metab.* 2011;22(9):374-81.
22. Huang S, Xing Y, and Liu Y. Emerging roles for the ER stress sensor IRE1alpha in metabolic regulation and disease. *The Journal of biological chemistry.* 2019;294(49):18726-41.

23. Le Grand F, and Rudnicki M. Satellite and stem cells in muscle growth and repair. *Development.* 2007;134(22):3953-7.

24. Tedesco FS, Dellavalle A, Diaz-Manera J, Messina G, and Cossu G. Repairing skeletal muscle: regenerative potential of skeletal muscle stem cells. *J. Clin. Invest.* 2010;120(1):11-9.

25. Ten Broek RW, Grefte S, and Von den Hoff JW. Regulatory factors and cell populations involved in skeletal muscle regeneration. *J. Cell. Physiol.* 2010;224(1):7-16.

26. Brack AS, and Rando TA. Tissue-specific stem cells: lessons from the skeletal muscle satellite cell. *Cell Stem Cell.* 2012;10(5):504-14.

27. Relaix F, and Zammit PS. Satellite cells are essential for skeletal muscle regeneration: the cell on the edge returns centre stage. *Development.* 2012;139(16):2845-56.

28. Yin H, Price F, and Rudnicki MA. Satellite cells and the muscle stem cell niche. *Physiological reviews.* 2013;93(1):23-67.

29. Liu N, et al. A Twist2-dependent progenitor cell contributes to adult skeletal muscle. *Nat. Cell Biol.* 2017;19(3):202-13.

30. Egerman MA, and Glass DJ. Signaling pathways controlling skeletal muscle mass. *Critical reviews in biochemistry and molecular biology.* 2014;49(1):59-68.

31. Ruegg MA, and Glass DJ. Molecular mechanisms and treatment options for muscle wasting diseases. *Annu. Rev. Pharmacol. Toxicol.* 2011;51(373-95.

32. Cohen S, Nathan JA, and Goldberg AL. Muscle wasting in disease: molecular mechanisms and promising therapies. *Nat. Rev. Drug Discov.* 2015;14(1):58-74.

33. Chamberlain JS, et al. Expression of the murine Duchenne muscular dystrophy gene in muscle and brain. *Science.* 1988;239(4846):1416-8.

34. Hoffman EP, Brown RH, Jr., and Kunkel LM. Dystrophin: the protein product of the Duchenne muscular dystrophy locus. *Cell.* 1987;51(6):919-28.

35. Liu Y, et al. Role for the endoplasmic reticulum stress sensor IRE1alpha in liver regenerative responses. *Journal of hepatology.* 2015;62(3):590-8.

36. Xu T, et al. The IRE1alpha-XBP1 pathway regulates metabolic stress-induced compensatory proliferation of pancreatic beta-cells. *Cell Res.* 2014;24(9):1137-40.

37. Yan Z, et al. Highly coordinated gene regulation in mouse skeletal muscle regeneration. *J. Biol. Chem.* 2003;278(10):8826-36.

38. Shao M, et al. Hepatic IRE1alpha regulates fasting-induced metabolic adaptive programs through the XBP1s-PPARalpha axis signalling. *Nature communications.* 2014;5(3528.

39. Rebbapragada A, Benchabane H, Wrana JL, Celeste AJ, and Attisano L. Myostatin signals through a transforming growth factor beta-like signaling pathway to block adipogenesis. *Molecular and cellular biology.* 2003;23(20):7230-42.

40. Liu L, Cheung TH, Charville GW, and Rando TA. Isolation of skeletal muscle stem cells by fluorescence-activated cell sorting. *Nature protocols.* 2015;10(10):1612-24.

41. Qiu Y, et al. A crucial role for RACK1 in the regulation of glucose-stimulated IRE1alpha activation in pancreatic beta cells. *Science signaling.* 2010;3(106):ra7.

42. Lee SJ. Regulation of muscle mass by myostatin. *Annual review of cell and developmental biology.* 2004;20(61-86.

43. Trendelenburg AU, Meyer A, Rohner D, Boyle J, Hatakeyama S, and Glass DJ. Myostatin reduces Akt/TORC1/p70S6K signaling, inhibiting myoblast differentiation and myotube size. *Am. J. Physiol. Cell Physiol.* 2009;296(6):C1258-70.

44. Rodgers BD, Wiedeback BD, Hoversten KE, Jackson MF, Walker RG, and Thompson TB. Myostatin stimulates, not inihibits, C2C12 myoblast proliferation. *Endocrinology.* 2014;155(3):670-5.

45. Wang L, Huang Y, Wang X, and Chen Y. Label-Free LC-MS/MS Proteomics Analyses Reveal Proteomic Changes Accompanying MSTN KO in C2C12 Cells. *BioMed research international.* 2019;2019(7052456.

46. Lee SJ, and McPherron AC. Regulation of myostatin activity and muscle growth. *Proceedings of the National Academy of Sciences of the United States of America.* 2001;98(16):9306-11.

47. Thies RS, et al. GDF-8 propeptide binds to GDF-8 and antagonizes biological activity by inhibiting GDF-8 receptor binding. *Growth factors.* 2001;18(4):251-9.

48. Hill JJ, et al. The myostatin propeptide and the follistatin-related gene are inhibitory binding proteins of myostatin in normal serum. *The Journal of biological chemistry.* 2002;277(43):40735-41.

49. Qiao C, et al. Myostatin propeptide gene delivery by adeno-associated virus serotype 8 vectors enhances muscle growth and ameliorates dystrophic phenotypes in mdx mice. *Human gene therapy.* 2008;19(3):241-54.

50. Mouisel E, et al. Myostatin is a key mediator between energy metabolism and endurance capacity of skeletal muscle. *American journal of physiology. Regulatory, integrative and comparative physiology.* 2014;307(4):R444-54.

51. Cross BC, et al. The molecular basis for selective inhibition of unconventional mRNA splicing by an IRE1-binding small molecule. *Proc. Natl. Acad. Sci. U. S. A.* 2012;109(15):E869-78.

52. Volkmann K, et al. Potent and selective inhibitors of the inositol-requiring enzyme 1 endoribonuclease. *J. Biol. Chem.* 2011;286(14):12743-55.

53. Wallace GQ, and McNally EM. Mechanisms of muscle degeneration, regeneration, and repair in the muscular dystrophies. *Annu. Rev. Physiol.* 2009;71(37-57.

54. Bentzinger CF, Wang YX, and Rudnicki MA. Building muscle: molecular regulation of myogenesis. *Cold Spring Harb. Perspect. Biol.* 2012;4(2).

55. Rodriguez J, et al. Myostatin and the skeletal muscle atrophy and hypertrophy signaling pathways. *Cellular and molecular life sciences : CMLS.* 2014;71(22):4361-71.

56. Bogdanovich S, et al. Functional improvement of dystrophic muscle by myostatin blockade. *Nature.* 2002;420(6914):418-21.

57. Murphy KT, et al. Antibody-directed myostatin inhibition improves diaphragm pathology in young but not adult dystrophic mdx mice. *The American journal of pathology.* 2010;176(5):2425-34.

58. Xiong G, et al. The PERK arm of the unfolded protein response regulates satellite cell-mediated skeletal muscle regeneration. *Elife.* 2017;6(

59. McCroskery S, Thomas M, Maxwell L, Sharma M, and Kambadur R. Myostatin negatively regulates satellite cell activation and self-renewal. *J. Cell Biol.* 2003;162(6):1135-47.

60. Rios R, Carneiro I, Arce VM, and Devesa J. Myostatin regulates cell survival during C2C12 myogenesis. *Biochem. Biophys. Res. Commun.* 2001;280(2):561-6.

61. Wu Y, et al. Dual role for inositol-requiring enzyme 1alpha in promoting the development of hepatocellular carcinoma during diet-induced obesity in mice. *Hepatology.* 2018;68(2):533-46.

62. Zhu H, et al. STAT3 Regulates Self-Renewal of Adult Muscle Satellite Cells during Injury-Induced Muscle Regeneration. *Cell Rep.* 2016;16(8):2102-15.

63. Grobet L, et al. A deletion in the bovine myostatin gene causes the double-muscled phenotype in cattle. *Nat. Genet.* 1997;17(1):71-4.

64. Lin J, Arnold HB, Della-Fera MA, Azain MJ, Hartzell DL, and Baile CA. Myostatin knockout in mice increases myogenesis and decreases adipogenesis. *Biochem. Biophys. Res. Commun.* 2002;291(3):701-6.

65. McPherron AC, Lawler AM, and Lee SJ. Regulation of skeletal muscle mass in mice by a new TGF-beta superfamily member. *Nature.* 1997;387(6628):83-90.

## Figures legends

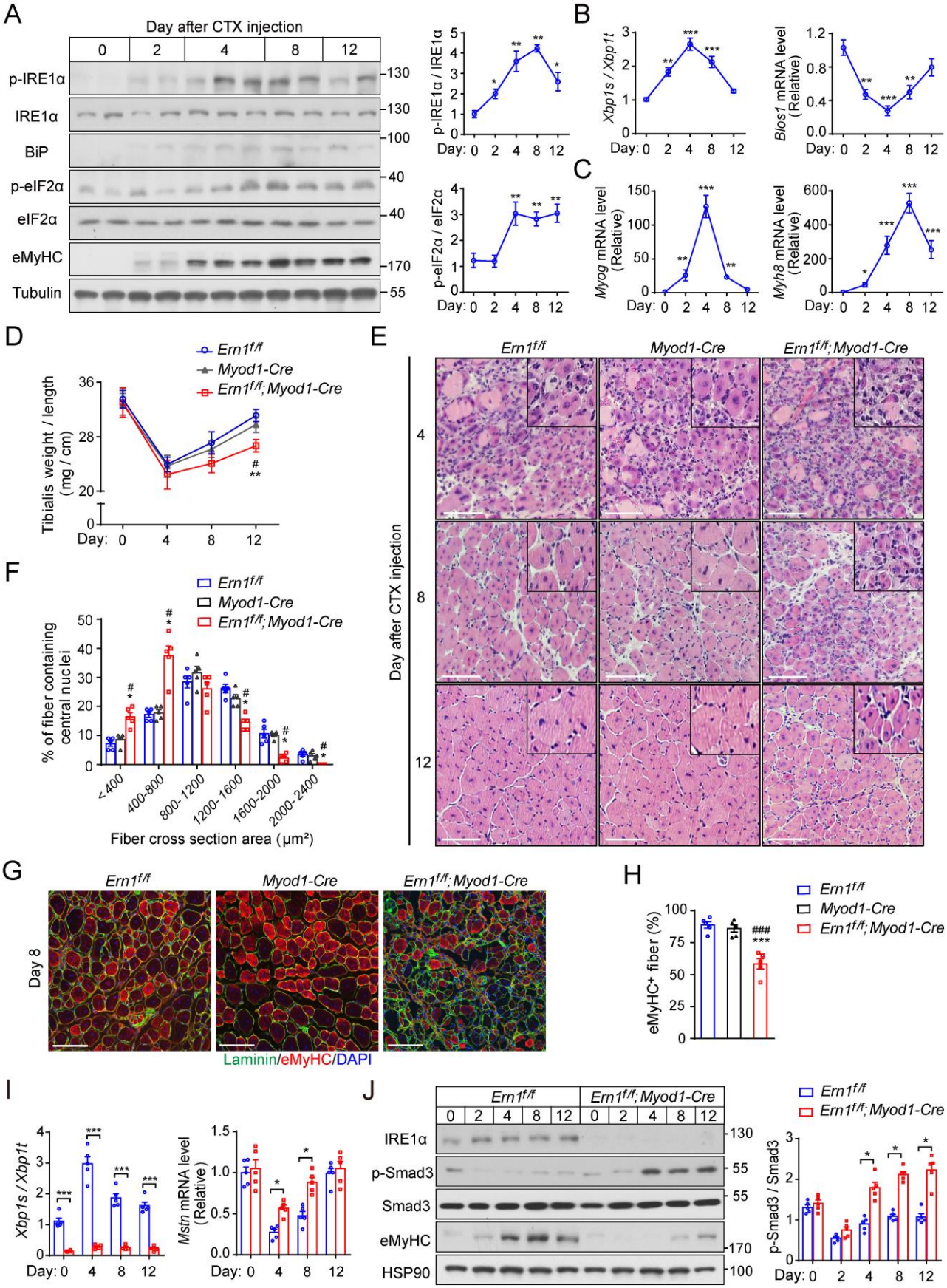

**Figure 1. Injury-induced IRE1α activation affects skeletal muscle regeneration and Myostatin signaling. (A-C)** Muscle injury induces IRE1α activation. Tibialis anterior (TA) muscle of adult male mice was injected with cardiotoxin (CTX) to induce acute muscle injury (n = 5 mice at each time point). **(A)** Immunoblot analysis of the phosphorylation of IRE1α and eIF-2α, and protein expression of BiP and eMyHC in muscle extracts. Each lane represents one individual mouse. Averaged p-IRE1α/IRE1α and p-eIF2α/eIF2α ratios are shown from densitometric quantification. **(B, C)** Quantitative RT-PCR analysis of *Xbp1* mRNA splicing and the abundance of mRNAs encoding the indicated genes. **(D-J)** IRE1α abrogation impairs muscle regeneration and enhances Myostatin signaling. TA muscles of male *Ern1*$^{f/f}$ and *Myod1-Cre* control and *Ern1*$^{f/f}$*;Myod1-Cre* mice were subjected to CTX-induced injuries (n = 5 mice at each time point). **(D)** The TA muscle weight relative to tibia length. **(E)** Representative H&E staining of TA muscles from mice of the indicated genotypes. **(F)** Percentage of regenerated myofibers in the indicated cross-sectional areas of TA muscles at 12 days after CTX injection. Myofibers containing centralized nuclei were quantified by ImageJ from 500 myofibers of the TA muscle in each mouse. **(G)** Representative Laminin (green) and eMyHC (red) immunostaining of TA muscles at 8 days after CTX injection. **(H)** Quantification of the percentage of eMyHC$^+$ myofibers within Laminin staining. **(I)** Quantitative RT-PCR analysis of *Xbp1* mRNA splicing and *Mstn* mRNA abundance in TA muscles. Data are shown as relative to the value for *Ern1*$^{f/f}$ TA muscle at day 0 after normalization to *Gapdh* as the internal control. **(J)** Immunoblot analysis of TA muscle lysates. Averaged p-Smad/Smad ratios are shown after normalization to the value for *Ern1*$^{f/f}$ TA muscle at day 0. All data are presented as the mean ± SEM. Significance was calculated by 1-way ANOVA **(A, B, C, H)** or 2-way ANOVA **(D, F, I, J)** with Bonferroni's multiple comparisons test. $^{*}P < 0.05$, $^{**}P < 0.01$, $^{***}P < 0.001$ relative to day 0 or *Ern1*$^{f/f}$. $^{\#}P < 0.05$, $^{\#\#\#}P < 0.001$ relative to *Myod1-cre*. Scale bars: 100 μm.

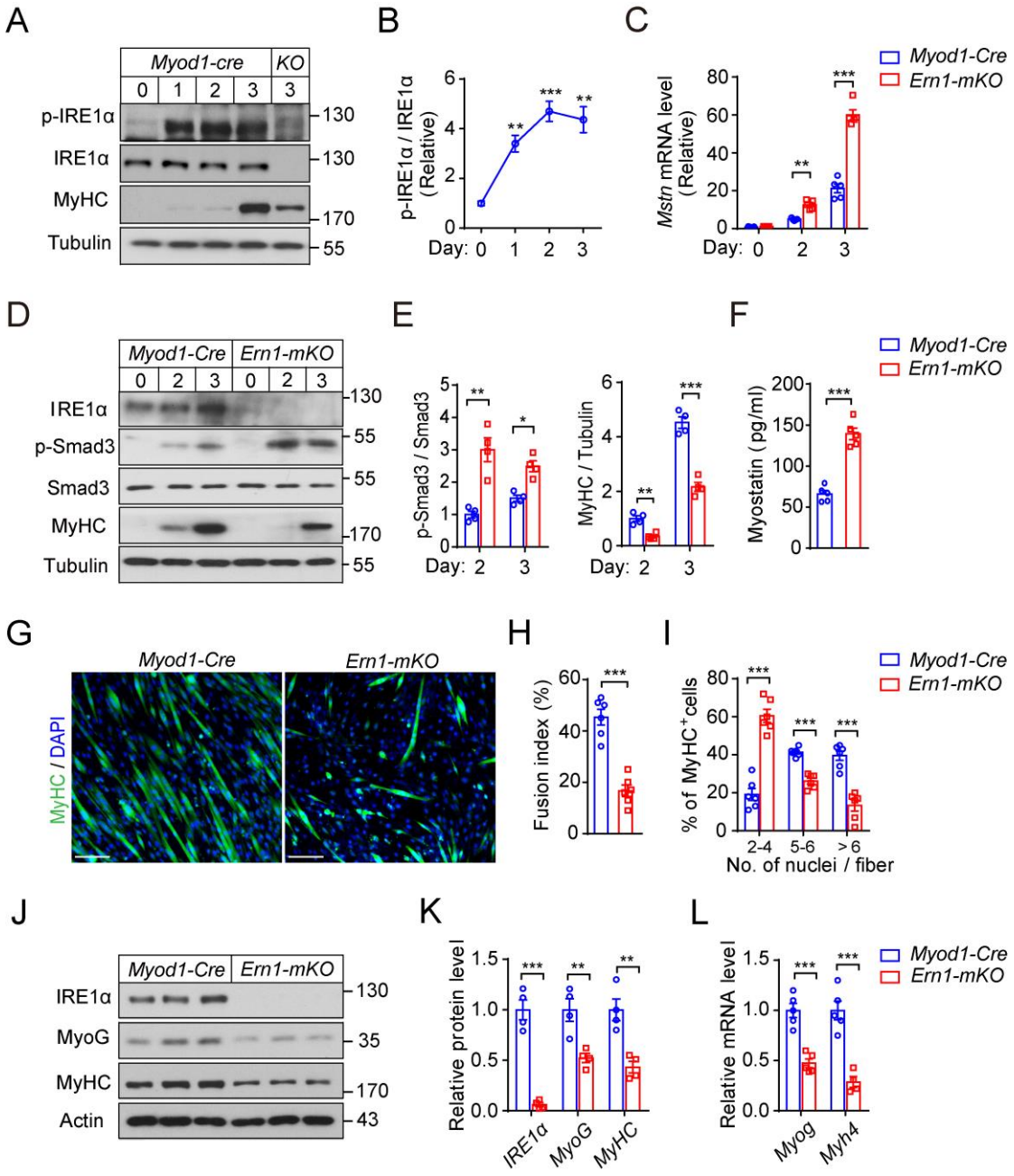


**Figure 2. IRE1α ablation increases Myostatin expression and impairs myoblast differentiation.** (**A-E**) Primary myoblasts isolated from TA muscle of male *Myod1-cre* and *Ern1*$^{f/f}$*;Myod1-Cre* (*KO* or *Ern1-mKO*) mice were differentiated for up to 3 days as indicated (n = 3-5 independent experiments). **(A, B)** Immunoblot analysis of IRE1α phosphorylation and MyHC expression **(A)** at the indicated time of differentiation, and quantification of averaged p-IRE1α/IRE1α ratios **(B)** is shown. **(C)** Quantitative RT-PCR analysis of the mRNA abundance of *Mstn.* **(D**, **E)** Immunoblot analysis of cell lysates **(D)** using the indicated antibodies, and averaged p-Smad3/Smad3 and MyHC/Tubulin levels **(E)** were quantified. **(F-L)** Primary TA myoblasts were differentiated into myotubes for 3 days (n = 4-6 independent experiments). **(F)** ELISA analysis of Myostatin protein in

culture medium. **(G-I)** Representative images **(G)** of immunostaining of Myosin heavy chain (MyHC, green) and DAPI staining of nuclei (blue). The fusion index **(H)** and the number of nuclei per $MyHC^+$ fiber **(I)** were quantified. **(J-L)** Immunoblot analysis **(J)** and quantification **(K)** of MyoG and MyHC in differentiated myocytes, and quantitative RT-PCR analysis **(L)** of their mRNA expression levels. All data are presented as the mean ± SEM. Significance was calculated by unpaired two-tailed Student's t-test **(F, H, I, K, L)**, 1-way ANOVA **(B)** or 2-way ANOVA **(C, E)** with Bonferroni's multiple comparisons test. $^{*}P < 0.05$, $^{**}P < 0.01$, $^{***}P < 0.001$ relative to *Myod1-Cre* group, or to day 0 for **(B)**. Scale bars: 100 μm.

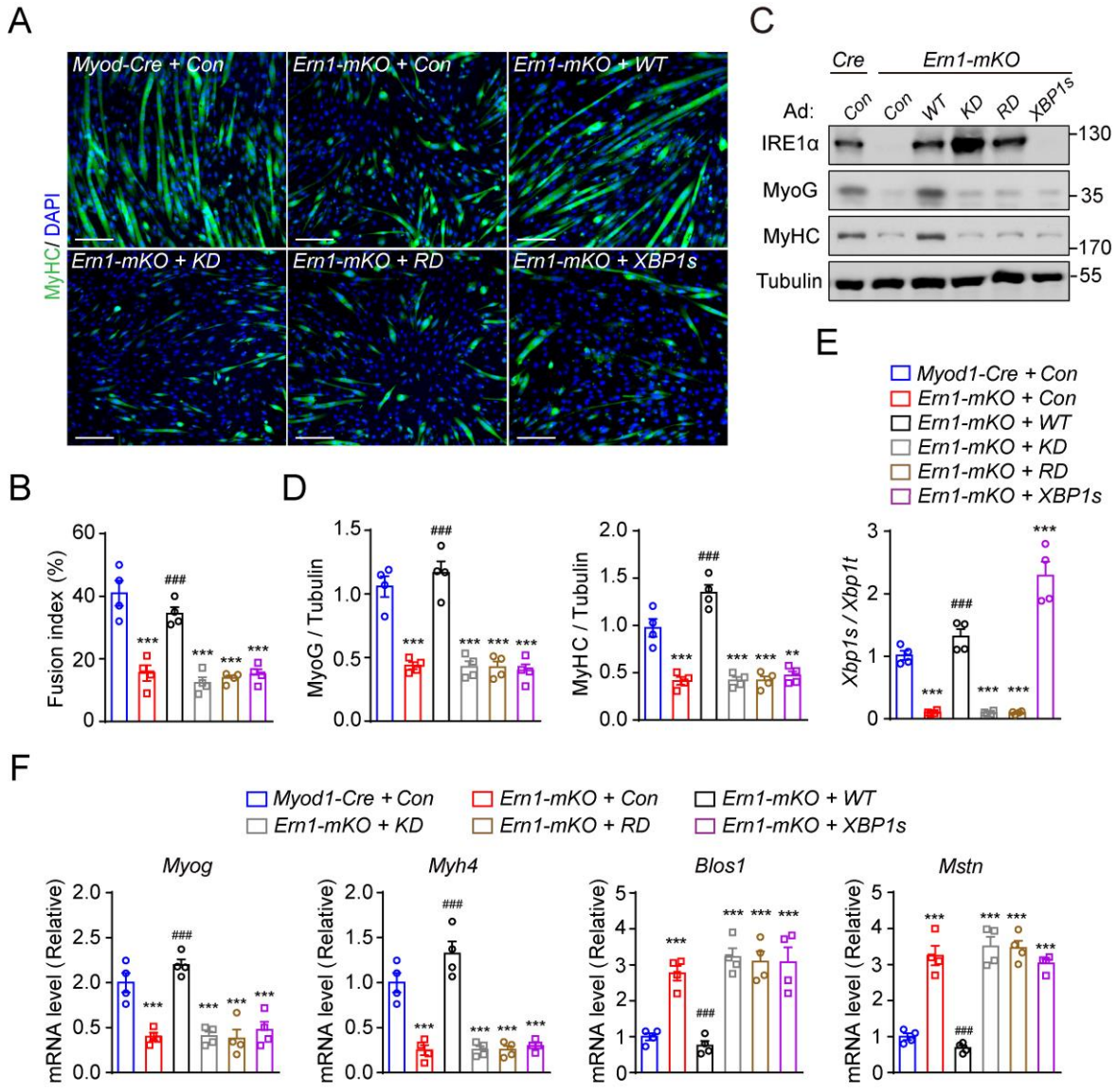


**Figure 3. IRE1α RNase blunts Myostatin signaling and promotes myoblast differentiation.** **(A-F)** Primary *Myod1-Cre* and *Ern1-mKO* myoblasts were infected with control recombinant adenovirus or adenoviruses expressing human wild-type (WT) or mutant (KD, kinase dead; RD, RNase dead) IRE1α protein or XBP1s and then differentiated for 3 days (n = 4 independent experiments). **(A)** Representative images of anti-MyHC and DAPI staining. **(B)** Quantification of the fusion index. **(C)** Immunoblot analysis of the indicated proteins. **(D)** Quantification of MyoG/Tubulin and MyHC/Tubulin after normalization to the value of control. **(E-F)** Quantitative RT-PCR analysis of *Xbp1* mRNA splicing **(E)** and the mRNA abundance of the indicated genes **(F)**. All data are presented as the mean ± SEM. Significance was calculated by 1-way ANOVA with Bonferroni's multiple comparisons test. $^{**}P < 0.01$, $^{***}P < 0.001$ relative to *Myod1-Cre* group. $^{\#\#\#}P < 0.001$ relative to *Ern1-mKO* + control adenovirus. Scale bars: 100 μm.

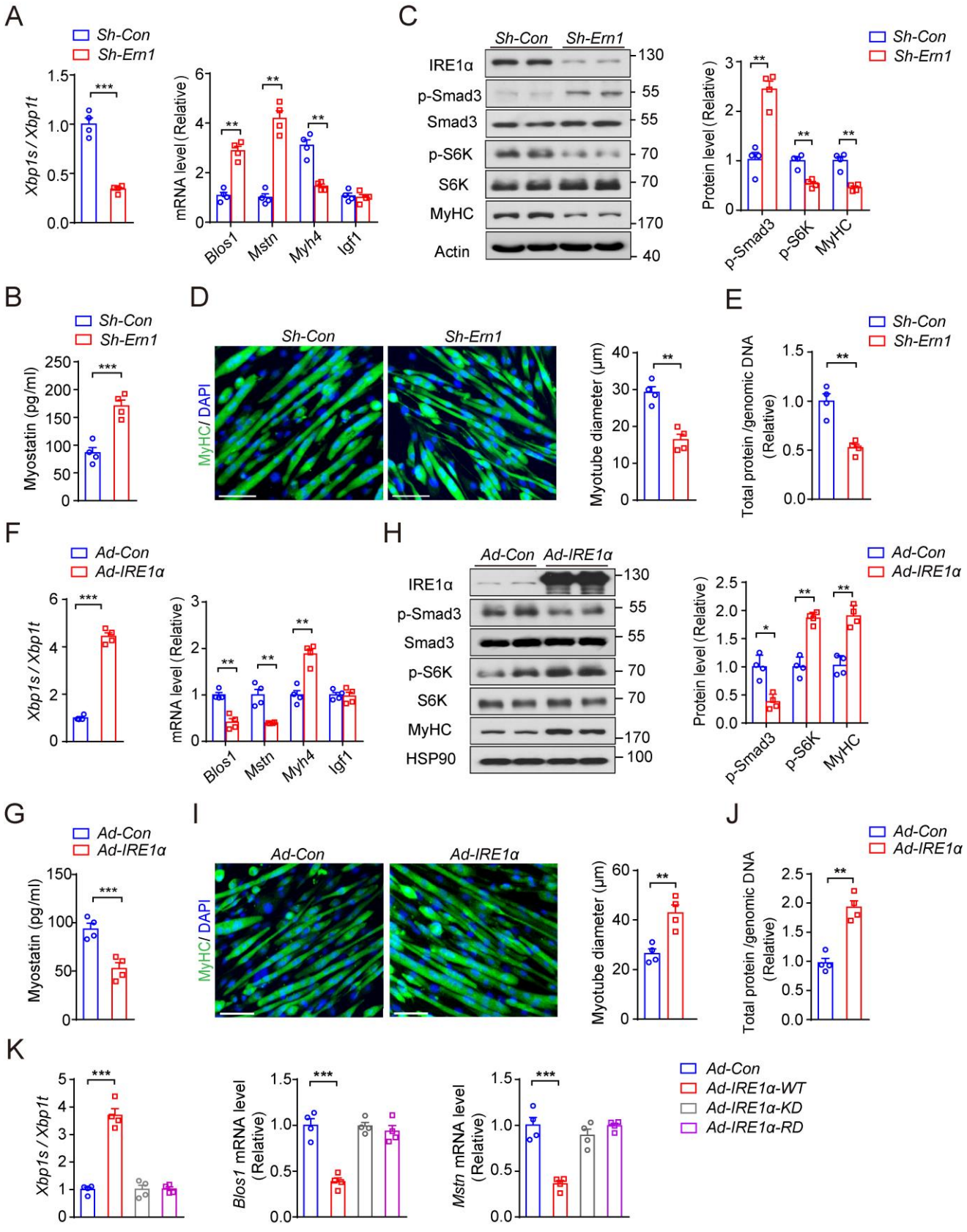


**Figure 4. IRE1α downregulates Myostatin expression and promotes hypertrophy of differentiated myotubes. (A-J)** C2C12 myoblast cells were differentiated for 4 days into myotubes

and then infected for 48 hours with **(A-E)** adenoviruses expressing a scramble control shRNA (Sh-Con) or shRNA directed against IRE1α (Sh-Ern1), or **(F-J)** empty control adenovirus or that expressing human IRE1α (n = 4 independent experiments). **(A, F)** Quantitative RT-PCR analysis of *Xbp1* mRNA splicing and the mRNA abundance of the indicated genes. **(B, G)** ELISA analysis of Myostatin protein in culture medium. **(C, H)** Immunoblot analysis of the indicated proteins from myotube extracts. Averaged MyHC/Actin, p-S6K/S6K and p-Smad3/Smad3 ratios were normalized to the value of Sh-Con or Ad-Con myotubes. **(D, I)** MyHC immunostaining of myotubes. Myotube diameters were quantified using ImageJ software. **(E, J)** Total cellular protein content relative to genomic DNA was measured in myotubes. **(K)** C2C12 myotubes were infected with empty control or adenoviruses expressing the WT or indicated mutant IRE1α protein. Quantitative RT-PCR analysis of *Xbp1* mRNA splicing and the mRNA abundance of *Blos1* and *Mstn* (n = 4 independent experiments). All data represent the mean ± SEM. Significance was calculated by unpaired two-tailed Student's t-test **(A-I)** or 1-way ANOVA **(K)** with Bonferroni's multiple comparisons test. $^{*}P < 0.05$, $^{**}P < 0.01$, $^{***}P < 0.001$ relative to Sh-Con or Ad-Con. Scale bars: 100 μm.

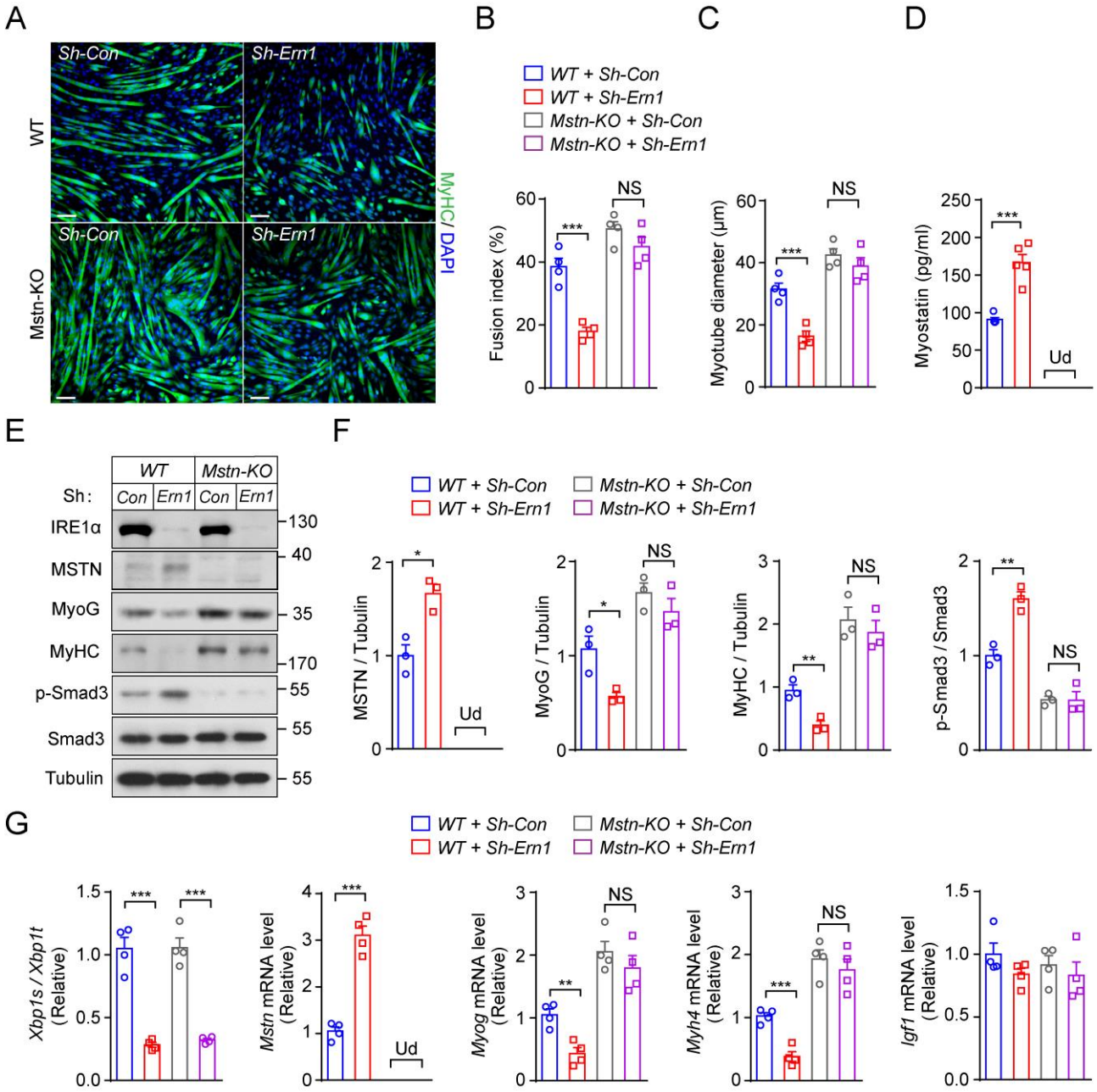


**Figure 5. Myostatin ablation reverses the effect of IRE1α deficiency on muscle cell differentiation and growth.** Wild-type (WT) and Mstn-KO C2C12 myoblast cells were infected for 24 hours with Sh-Con or Sh-Ern1 adenoviruses and then differentiated for 3-4 days in myogenic medium. **(A-C)** Representative images of MyHC immunostaining **(A)**, and quantification of the fusion index **(B)** and myotube diameters **(C)** (n = 4 independent experiments). **(D)** ELISA analysis of Myostatin protein in culture medium (n = 3 independent experiments). **(E, F)** Immunoblot analysis of the indicated proteins **(E)**, and quantification of averaged MSTN/Tubulin, MyoG/Tubulin, MyHC/Tubulin and p-Smad3/Smad3 levels **(F)** (n = 3 independent experiments). **(G)** Quantitative RT-PCR analysis of *Xbp1* mRNA splicing and the mRNA abundance of the indicated genes (n = 4

independent experiments). All results represent the mean ± SEM. $^{*}P < 0.05$, $^{**}P < 0.01$, $^{***}P < 0.001$ by 2-way ANOVA with Bonferroni's multiple comparisons test. NS, no significance; Ud, undetectable. Scale bars: 100 μm.

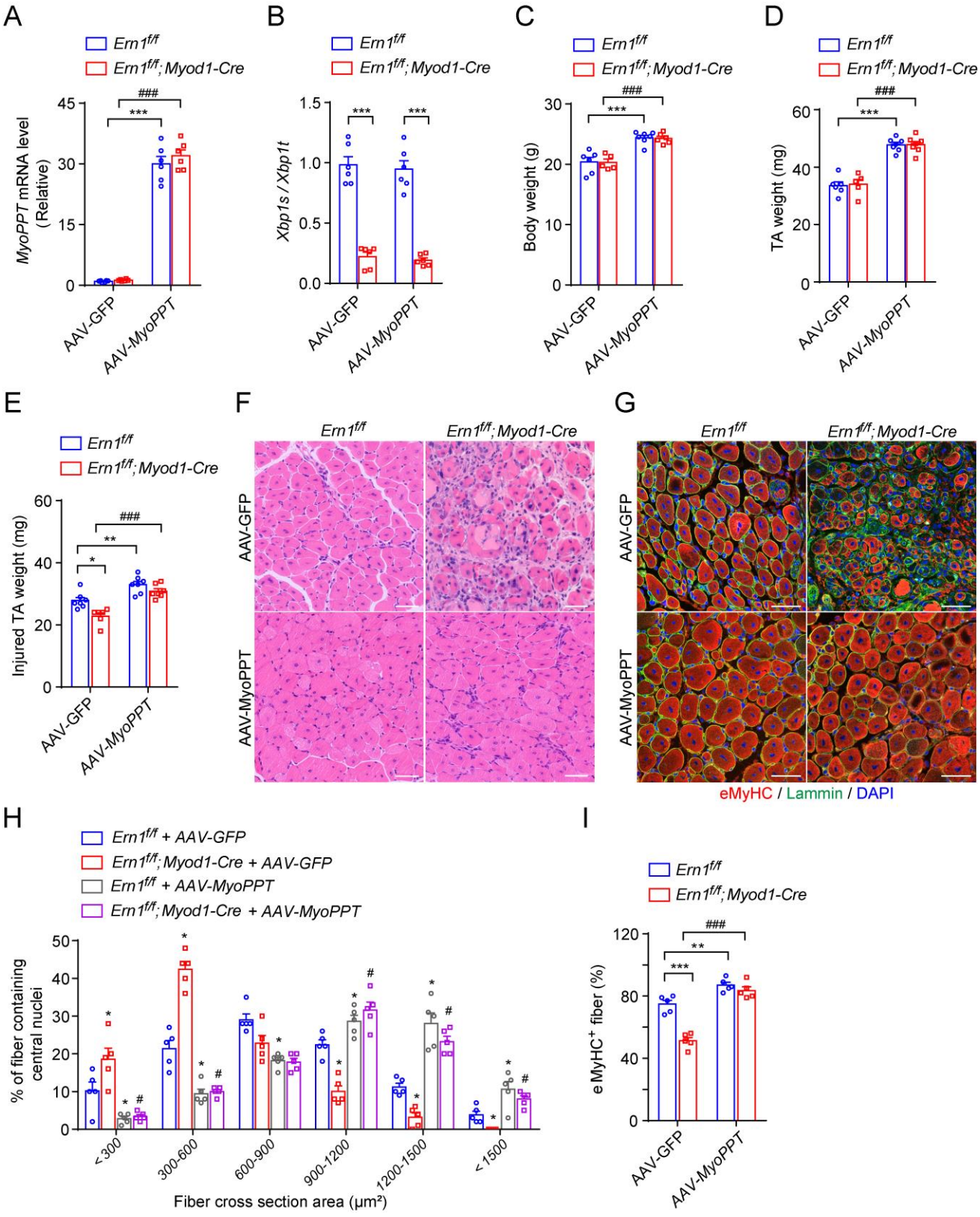


**Figure 6. Inhibition in vivo of Myostatin signaling rescues the impairment of muscle regeneration resulting from IRE1α deficiency.** Male *Ern1*$^{f/f}$ or *Ern1*$^{f/f}$;*Myod1-Cre* mice were injected intraperitoneally on postnatal day 3 (P3) and day 6 (P6) with adeno-associated virus 2/9 (AAV2/9) expressing GFP (AAV-GFP) or MyoPPT (AAV-MyoPPT). TA muscles of indicated mice

were injected with PBS or CTX at 7 weeks of age and analyzed at 8 days after injection. **(A, B)** Quantitative RT-PCR analysis of the mRNA abundance of *MyoPPT* **(A)** and *Xbp1* mRNA splicing **(B)** in PBS-treated uninjured TA muscles (n = 6 mice per group). **(C)** Body weight from mice of the indicated groups, **(D)** Weight of PBS-treated uninjured TA muscles, **(E)** Weight of CTX-injured TA muscles from mice of the indicated groups (n = 5-7 mice per group). Representative H&E staining **(F)**, Laminin (green) and eMyHC (red) immunostaining **(G)** of injured TA muscles (n = 5 mice per group). **(H)** Percentage of regenerated myofibers in the indicated cross-sectional areas of TA muscles. Myofibers containing centralized nuclei were quantified by ImageJ from 500 myofibers in each mouse (n = 5 mice per group). **(I)** Quantification of the percentage of $eMyHC^{+}$ myofibers within Laminin staining (n = 5 mice per group). All data are presented as the mean ± SEM. Significance was calculated by 2-way ANOVA with Bonferroni's multiple comparisons test. $^{*}P < 0.05$, $^{**}P < 0.01$, $^{***}P < 0.001$ relative to $Ern1^{f/f}$+AAV-GFP. $^{\#}P < 0.05$, $^{\#\#\#}P < 0.001$ relative to $Ern1^{f/f}$;*Myod1-Cre* +AAV-GFP. Scale bars: 100 μm.

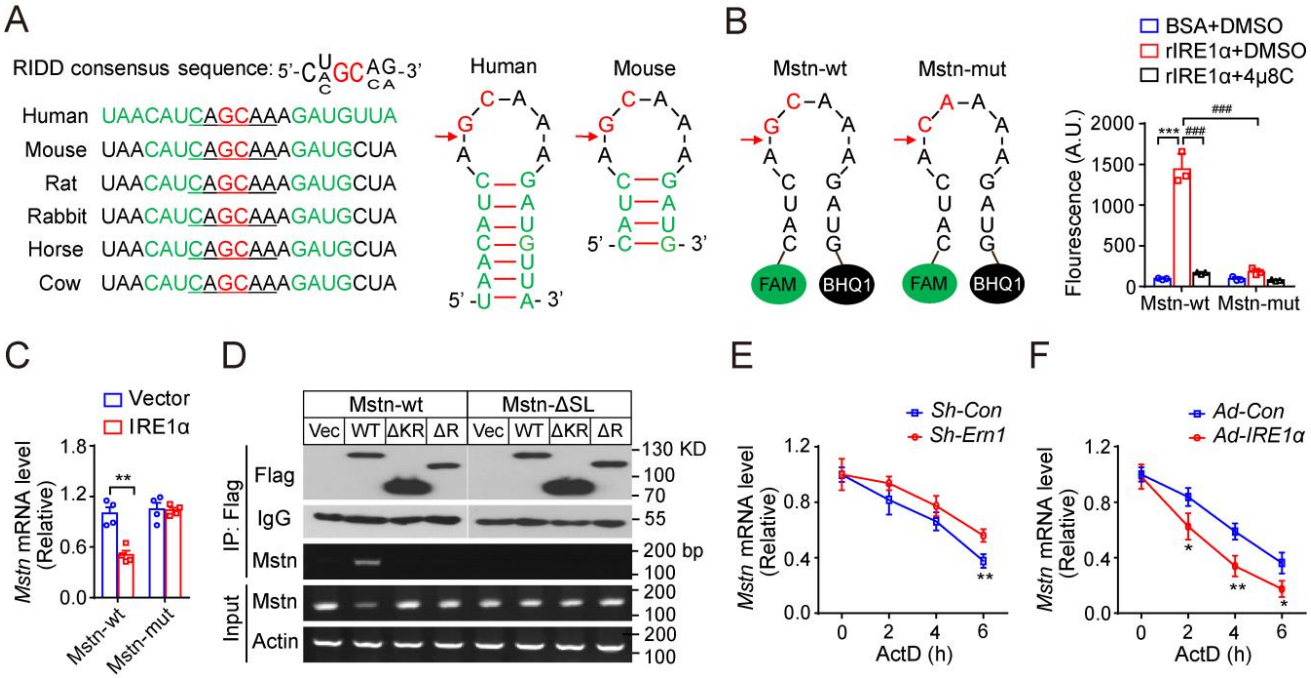


**Figure 7.** ***Myostatin mRNA is an RIDD target of IRE1α.*** **(A)** Sequence alignment of *Mstn* mRNAs from the indicated species with the putative conserved RIDD region, with the predicted stem-loop secondary structure shown for human and mouse *Mstn* mRNA. The potential IRE1α cleavage site is indicated by the arrow. **(B)** Fluorescence-based analysis of IRE1α cleavage of the synthetic wild-type (wt) or mutant (mut, GC to CA) *Mstn* mRNA (n = 3 independent experiments). **(C)** Quantitative RT-PCR analysis of the abundance of *Mstn* mRNA in HEK293T cells co-transfected with plasmids expressing the entire coding region of WT or mutant Myostatin (GC to CA) together with empty vector or human IRE1α expression plasmid (n = 4 independent experiments). **(D)** HEK293T cells were co-transfected with plasmids expressing the wt or stem-loop deletion (ΔSL) mutant Myostatin together with vector (Vec) control or plasmids expressing Flag-tagged human WT or deletion mutant (KR, kinase and RNase domain; R, RNase domain) IRE1α proteins. Representative RT-PCR analysis of *Mstn* mRNA from immunoprecipitates (IP) using anti-Flag antibody or from total cellular RNA (Input). Shown also are representative immunoblots of immunoprecipitated IRE1α proteins and IgG control (n = 3 independent experiments). **(E, F)** The stability of the *Mstn* mRNA was determined by quantitative RT-PCR in C2C12 myotubes infected with **(E)** Sh-Con or Sh-Ern1 adenoviruses, or **(F)** Ad-Con or Ad-IRE1α adenoviruses, after treatment with Actinomycin D (ActD) for the indicated time intervals. Data are shown relative to the value at time 0 of ActD treatment (set as 1) after normalization to the GAPDH mRNA level as internal control (n = 3 independent experiments). All data are shown as the mean ± SEM. Significance was calculated by 2-way ANOVA with Bonferroni's multiple comparisons test. $^{*}P < 0.05$, $^{**}P < 0.01$, $^{***}P < 0.001$, $^{\#\#\#}P<0.001$ Scale bars: 100 μm.

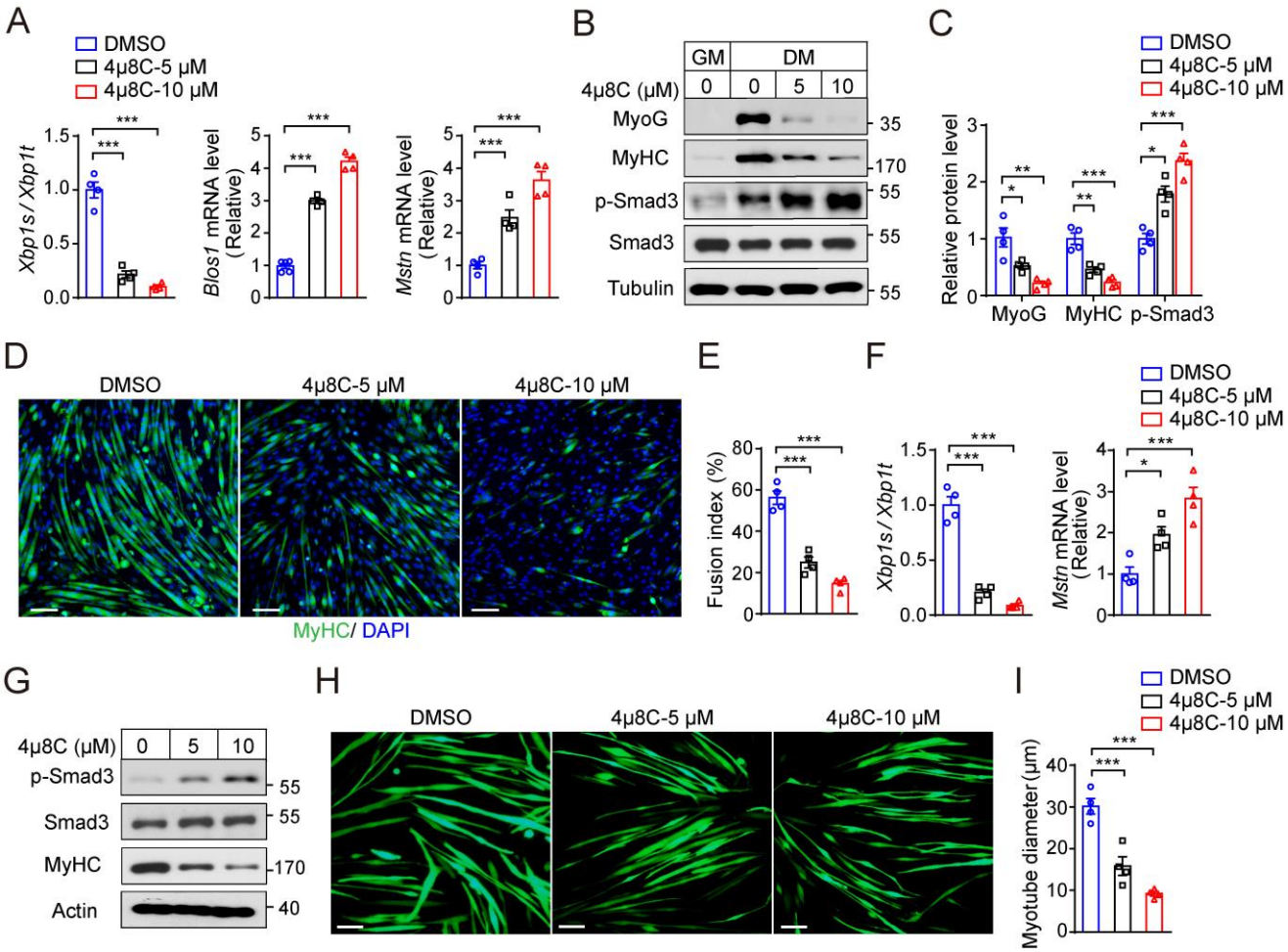


**Figure 8. Pharmacologic inhibition of IRE1α RNase activity impairs muscle cell differentiation and growth. (A-E)** Primary myoblasts isolated from WT mice were cultured in growth medium (GM), and subsequently incubated in differentiation medium (DM) with or without 4μ8C for 3 days (n = 4 independent experiments). **(A)** Quantitative RT-PCR analysis of *Xbp1* mRNA splicing and the mRNA abundance of *Blos1* and *Mstn*. **(B)** Immunoblot analysis of the expression of the indicated proteins, and **(C)** quantification of MyoG/Tubulin, MyHC/Tubulin and p-Smad3/Smad3 levels. **(D)** MyHC immunostaining, and **(E)** quantification of the fusion index. **(F, G)** Differentiated C2C12 myotubes were treated for 24 hours with DMSO versus 5 μM or 10 μM 4μ8C. **(F)** Quantitative RT-PCR analysis of *Xbp1* mRNA splicing and the *Mstn* mRNA abundance (n = 4 independent experiments). **(G)** Immunoblot analysis of the indicated proteins (n = 3 independent experiments). **(H, I)** C2C12 myoblasts infected by EGFP-expressing adenovirus were differentiated for 4 days and likewise treated with 4μ8C (n = 4 independent experiments). **(H)** Representative images of myotubes by fluorescence microscopy. **(I)** Quantification of myotube diameters using ImageJ software**.** All data are shown as the mean ± SEM. Significance was calculated by 1-way ANOVA with Bonferroni's multiple comparisons test and $^{*}P < 0.05$, $^{**}P < 0.01$, $^{***}P < 0.001$. Scale bars: 100 μm.

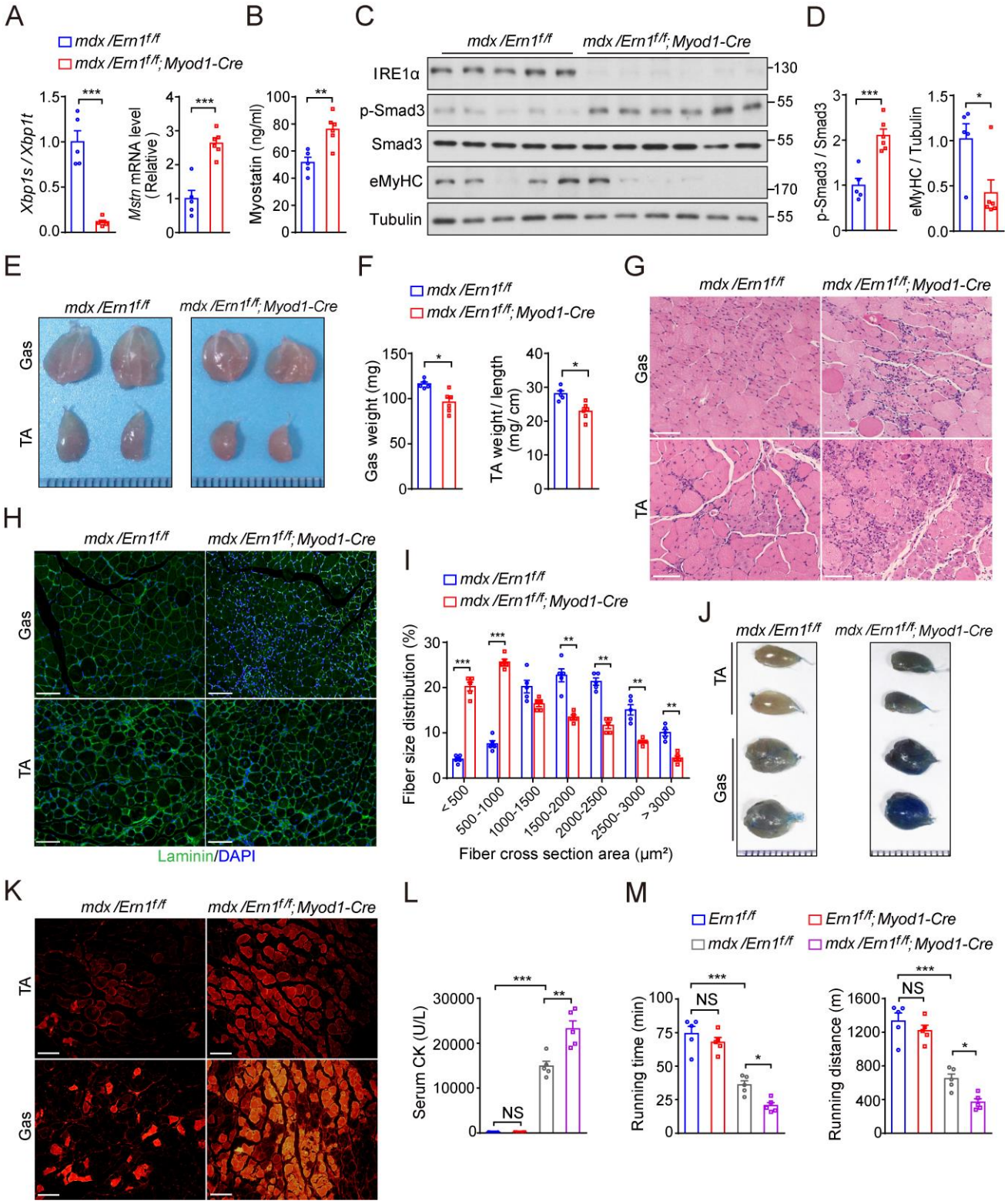


**Figure 9. Loss of IRE1α exacerbates the dystrophic phenotypes in *mdx* mice. (A)** Quantitative RT-PCR analysis of *Xbp1* mRNA splicing and the mRNA abundance of *Mstn* in TA muscles from male *mdx/Ern1*$^{f/f}$ and *mdx/Ern1*$^{f/f}$*;Myod1-Cre* mice at 6 weeks of age (n = 5-6 mice per genotype). **(B)** ELISA analysis of serum Myostatin levels (n = 5-6 mice per genotype). **(C)** Immunoblot analysis of

TA muscle lysates using the indicated antibodies, and **(D)** averaged p-Smad3/Smad3 and eMyHC/Tubulin ratios are shown after normalization to the value in *mdx* muscle (n = 5-6 mice per genotype). **(E, F)** Representative pictures **(E)** and weight **(F)** of gastrocnemius (Gas) and TA muscles from *mdx/Ern1*$^{f/f}$ and *mdx/Ern1*$^{f/f}$*;Myod1-Cre* mice at 6 weeks of age (n = 5-6 mice per genotype). **(G)** Representative images of H&E staining of Gas and TA muscles, and **(H)** Laminin (green) immunostaining of Gas and TA muscles (n = 5 mice per genotype). **(I)** Percentage of myofibers in the indicated cross-sectional areas of TA muscle. Quantification was conducted by ImageJ from 500 myofibers of the TA muscle from each mouse (n = 5 mice per genotype). **(J, K)** Analysis of Evans blue dye (EBD) uptake of Gas and TA muscles (n = 5 mice per genotype). **(J)** Representative images of Gas and TA muscles. **(K)** Representative fluorescent micrographs of muscle sections. **(L)** Serum creatine kinase (CK) activity, and **(M)** mean running time and distance on a motorized treadmill for mice of the indicated genotypes at 6 weeks of age (n = 5 mice per genotype). All data are shown as the mean ± SEM. Significance was calculated by unpaired two-tailed Student's t-test **(A, B, D, F)**, 2-way ANOVA **(I)** or 1-way ANOVA **(L, M)** with Bonferroni's multiple comparisons test. $^{*}P < 0.05$, $^{**}P < 0.01$, $^{***}P < 0.001$. Scale bars: 100 μm.

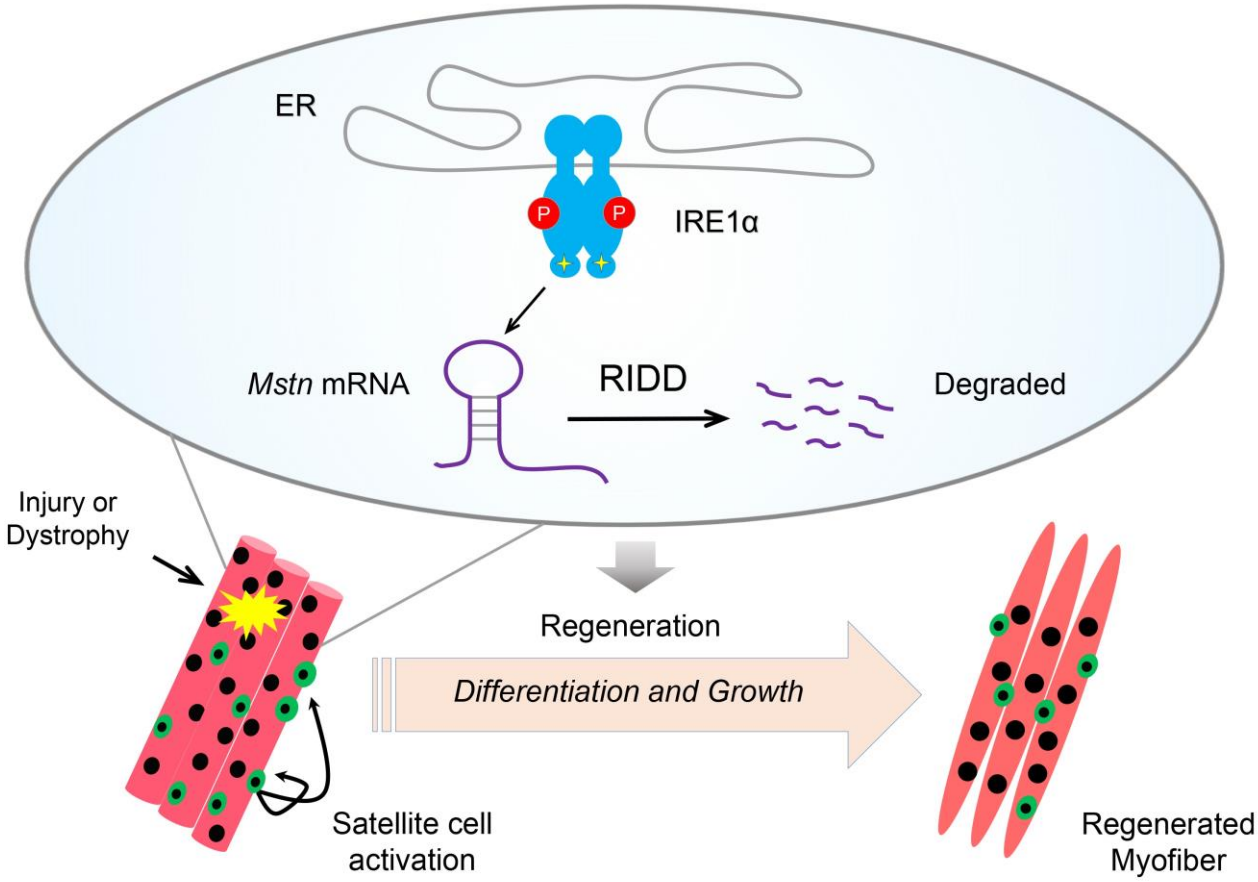


**Figure 10. IRE1α regulates skeletal muscle regeneration through RIDD suppression of Myostatin.** Upon injury-induced or dystrophy-associated stress, IRE1α RNase is activated in muscle cells to decay the mRNA encoding Myostatin, thereby promoting myoblast differentiation and myotube growth during the skeletal muscle regeneration response.